Nano Research

Open Access

Mini Review

Biomass materials for zinc-based sustainable and green energy storage devices: Strategy and mechanism

Xiaotong Yang[1,§], Xiaoxin Nie[1,§], Chenke Tang[2], Yiyang Xiao[2], Qiongguang Li[3], Du Yuan[1]✉, and Meng Yao[2]✉

[1] College of Materials Science and Engineering, Changsha University of Science and Technology, Changsha 410004, China
[2] College of Materials Science and Engineering, Sichuan University, Chengdu 610065, China
[3] Anhui Province International Research Center on Advanced Building Materials, School of Materials and Chemical Engineering, Anhui Jianzhu University, Hefei 230601, China
[§] Xiaotong Yang and Xiaoxin Nie contributed equally to this work.

Cite this article: *Nano Research*, **2025**, *18*, 94907031. https://doi.org/10.26599/NR.2025.94907031

ABSTRACT: As next-generation rechargeable alternatives, zinc-based energy storage devices (ZESs) are being intensely explored due to their merits of abundant resource, low cost, safety and environmental benignity. However, ZESs face a succession of critical challenges on pursuing advancing performance, including the stability and kinetics of cathode, stability and transport of zinc electrolyte, reversibility and deep utilization of metallic Zn anode. Biomass, possessing unique molecular structures with abundant functionals groups, motivates the interdisciplinary field emerging from biomass and aqueous rechargeable battery. Concerning its high compatibility with ZES design, we here summarize the application of biomass materials in ZESs from the aspects of cathode, electrolyte, membrane/separator and Zn anode, with their corresponding operational mechanisms and attractive functionalities from polymeric structures. Accordingly, the outlooks and perspectives are provided, regarding current challenges and future directions. We anticipate our minireview paves way on exploring the roles of biomass in aqueous rechargeable batteries.

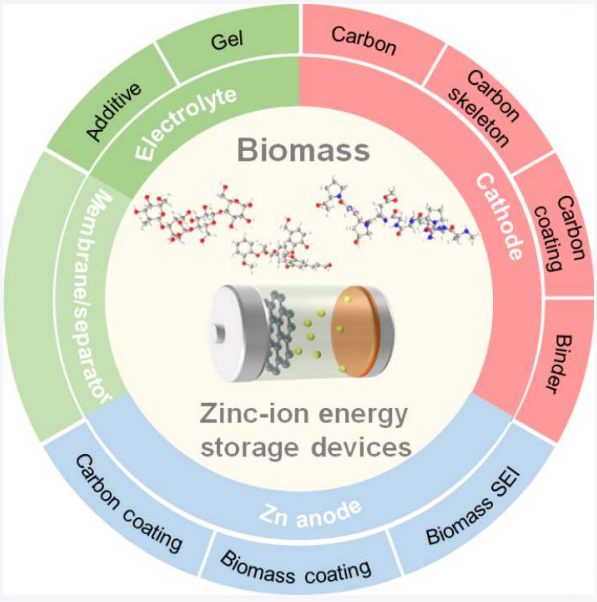

KEYWORDS: zinc, biomass materials, skeleton/host, coating, solid-electrolyte interphase (SEI)

1 Introduction

With increasingly severe resource depletion and environmental issues, the development of next-generation rechargeable alternatives beyond lithium-ion batteries are drawing intense attention [1–9]. As outstanding post-lithium candidates, aqueous zinc-based energy storage devices (ZESs) are intensely concerned, due to the merits of abundant resource, low cost, safety, environmental benignity and promising performance [10–13]. In ZESs, zinc ion batteries (ZIBs) consist of a cathode that is capable of storing/releasing Zn^{2+}/H^+ ions, an aqueous electrolyte for ion conduction and a metallic Zn anode holding good compatibility with aqueous electrolytes and permitting reversible Zn stripping/plating (−0.762 V vs. standard hydrogen electrode (SHE)) [14–16]. Additionally, compared with other metal anode candidates, Zn anode possesses high theoretical gravimetric and volumetric capacity of 820 mAh·g^{-1} and 5855 mAh·cm^{-3} [17–20]. In parallel, zinc ion capacitors (ZICs) can be constructed by coupling Zn anode with carbon-based materials, which possess the advantage of boosted kinetics and ultrastable cycling stability [21–23] .

However, the implementation of ZESs is hindered by a serial challenge arising from cathode, electrolyte, to Zn anode. The issues on the cathode materials in ZESs lies in their stability during cycling (e.g., dissolution of transition metal ions, collapse of layer structure, etc.) and sluggish kinetics due to limited ion conductivities in non-

Received: August 6, 2024; **Revised:** September 1, 2024
Accepted: September 12, 2024

✉Address correspondence to Du Yuan, aduyuandu@outlook.com; Meng Yao, yaomeng@scu.edu.cn

carbon materials [24]. Also, enlarging capacities for carbon-based cathodes are long-remaining problems in energy storage devices. Regarding electrolytes, water-induced reactions of hydrogen evolution and oxygen evolution restrict their electrochemical windows (EWs) [25–32], where a compromise between EWs and ion conductivities needs to be balanced when designing novel electrolytes. The design of ZESs is further troubled by the irreversibility of metallic Zn anode, low Coulombic efficiency (CE) and poor cyclic stability [33], which roots in the issues of dendrite growth, hydrogen evolution reaction (HER), corrosion and formation of surface by-products [13, 34–37]. A succession of strategies has been proposed to achieve stable Zn anodes, including structural design of Zn anode, regulation of the electrolyte–Zn interface and optimization of electrolyte [15, 38–42]. The methods of preparing advancing Zn anode include three-dimensional (3D) design, electrodeposition [43–45], alloy [46, 47] and mechanical/thermal treatments [48, 49]. By 3D design, specific surface area (SSA) of electrode can be enhanced with improved electrical conductivity, which allows electric field regulation and accommodation of volume change of Zn during cycling. By electrodeposition, the texture of metallic Zn can be manipulated. Specifically, Zn (002) texture can effectively prevent the dendrite growth, reduce the surface corrosion and promote reversible Zn deposition [43–45, 50, 51]. Surface coating/artificial solid-electrolyte interphase (SEI) can regulate ion diffusion, offer zincophilicity between the protective layer and Zn^{2+} and redistribute ionic concentration as well as local electrical field. Also, rational design of surface coating/SEI can prevent the direct contact between Zn and electrolyte, effectively depressing HER and surface corrosion [52–57]. Novel electrolytes including water-in-salt electrolytes, deep eutectic electrolytes (DESs), electrolyte additives, gel electrolytes and solid-state electrolytes are developed [58–67], which can alter zinc solvation structure, tune water activity and regulate interfacial chemistry on Zn, inhibiting HER and forming effective *in situ* SEI [33].

Biomass material, exist in living organisms in the form of biomolecules or carbohydrates with intricate chemical structures and multiple types of functional groups. They possess the characteristics towards a circular economy of natural abundance, cost-effectiveness, renewability, degradability, nontoxic and ecological benefits, which contribute to sustainable development, environmental friendliness and even safe production [68]. More than the above unique advantages, their physicochemical attributes are highly compatible with the design of aqueous batteries, which attract fast growing attention in ZESs. Natural polymers are rich in polar functional groups, which can offer favorable binding sites with metallic ions, reshaping the solvation structure of zinc ions. Meantime, the hydrophilicity of functional groups can tune the water activity. Further, the arrangement of functional groups from local environment towards long range network, can manipulate the ion transport behavior. Besides influencing the electrochemical behavior of electrolyte–electrode interface, the enriched molecule structures of biomass can bring the advantages such as flexibility, toughness and self-healing. Also, biomass materials can be facilely converted into advancing carbon nanostructures, functioning as hosts for charge storage or growth of active materials and protection layer. So far, there are few reviews focusing on the impact of biomass materials in ZESs. Therefore, it is imperative to explore the operational mechanisms of biomass materials in ZESs towards sustainability, especially for the key components including cathode, electrolyte, membrane/separator and Zn anode.

Generally, biomass can be classified into polysaccharides (rich in –OH), polyphenols (rich in ph–OH) and proteins. Polysaccharides include cellulose, semi-cellulose, chitosan ($–NH_2$), chitin (–CONH–), alginic acid (–COOH) and sodium alginate (SA) ($–COO^-$). Cellulose is the most abundant renewable natural biopolymer on earth and possesses outstanding mechanical properties, good thermal stability and excellent biocompatibility [69]. Polyphenols, include lignin, tannic acid (TA), gallic acid, etc. Lignin, a major component of lignocellulose, is the largest source of aromatic building blocks on the planet and harbors great potential to serve as starting material for the production of biobased products [70]. TA consists of numerous polar groups such as hydroxyl, which can be chelated with metallic ions. And as for proteins, gelatin, guar gum (GG), xanthan gum and carrageenan are included. Thereinto, gelatin, has been well-developed because of its good biocompatibility, biodegradability, easy processability, wide availability and low cost [71]. Importantly, functionalities of biopolymers are intimately correlated with their molecular nature, where a systematic discussion is acquired for the high-performance energy storage devices.

Herein, we expound the emerging roles of biomass materials in zinc-based energy storage devices (Fig. 1). Conversion of biomass into advancing carbon materials for energy storage is discussed, including their roles as cathodes, hosts or protective layers. The functions of biomass as natural polymeric integrities for the key entities in both ZIBs and ZICs are focused. The sections are developed based on the utilization strategies and working mechanisms of biomass for ZESs, from the aspects of cathodes, electrolytes, membranes/separators and artificial SEI/*in situ* SEI. Besides the above promising aspects, the use of biomass in ZESs faces the challenges of controllable synthetic microstructure and unclear operational mechanism, interplay between water and functional groups in complex electrolyte system with processing compatibility and complicated interfacial reactions on electrolyte-Zn. Hence, outlooks and perspectives on exploring the functions of biomass are provided to pursue high performance ZESs from the angles of microstructure regulation on cathode as well as operational mechanism study, physicochemical properties of electrolytes, chemistry on biomass-based electrolyte-Zn interface and multi-functionalities, towards the construction of reliable energy storage systems.

2 Biomass materials for cathodes in ZESs

Novel carbon nanostructures can be derived from biomass for cathode materials in ZESs (Fig. 2) [72]. Except for the inherited natural abundance, they offer large SSA, plentiful active sites and favorable conductivities. These features enable the assembled ZESs with outstanding electrochemical performance, including high capacity, superior power density and extraordinary cycle stability. In addition, biomass-derived carbons can work as skeletons for the growth of electrode materials and promote the reaction kinetics of electrode. When applied as protective layers for cathodes, interconnected porous structure of the derived carbons can provide internal tunnels to facilitate ion transport and improve electrical conductivity. In addition, biopolymers can be directly used as binders for cathodes, where the strong electron withdrawing functional groups in biomass, like carboxymethyl groups, can form strong H-bond with oxygen in cathodes to enhance their intimate contact. Moreover, biopolymers endow cathodes with a high degree of wettability and flexibility.

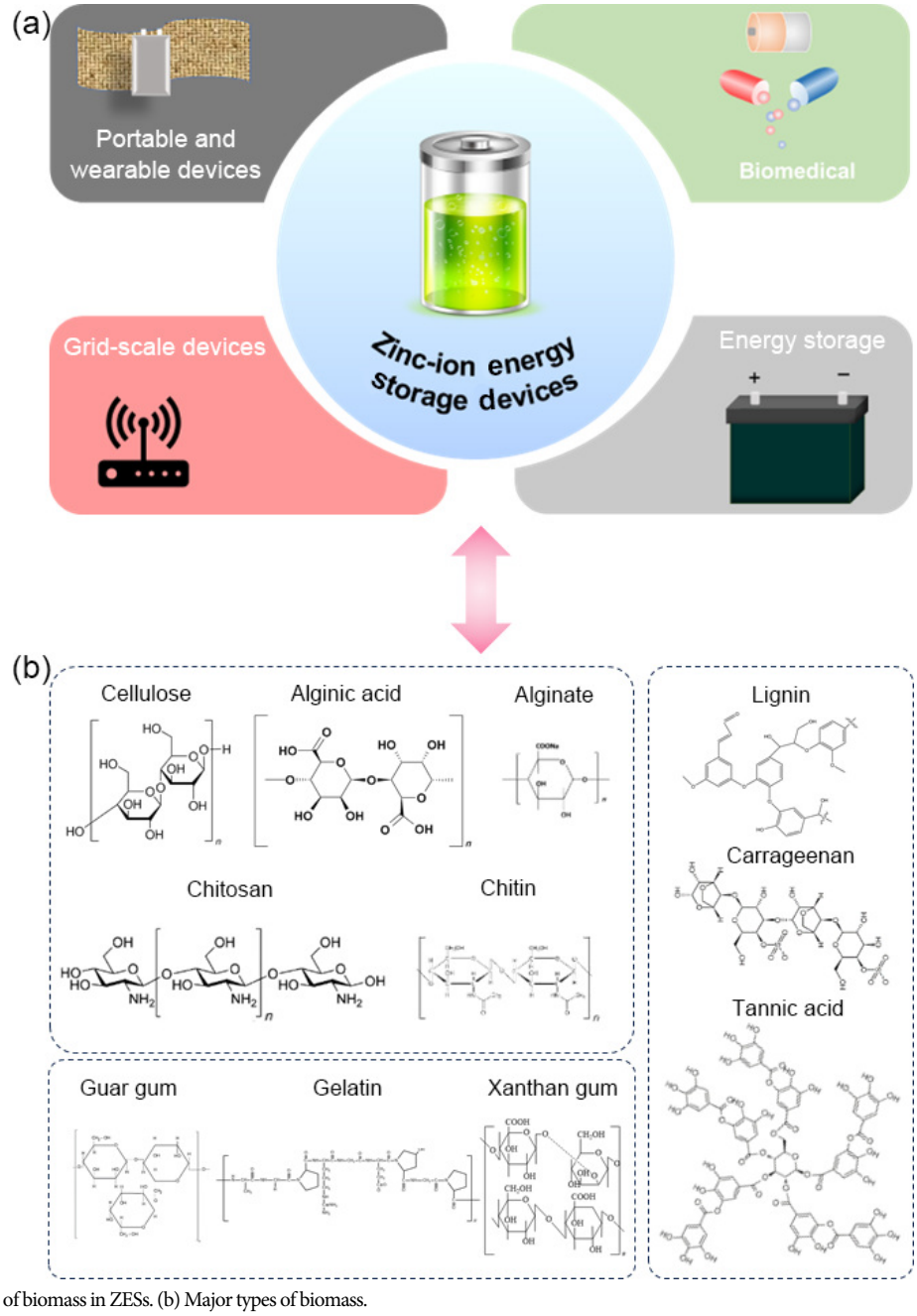

Figure 1 (a) Application of biomass in ZESs. (b) Major types of biomass.

2.1 Biomass-derived carbon materials as cathode materials

When converted into novel nanostructures, facile synthetic strategies have been developed for different categories of biomass. And the resulted features of derived carbons, including pore size/structure, surface area and active sites, are directly related to the charge storage performance in ZICs.

It is important to achieve the tuning of pore structure in biomass-derived carbon. A $ZnCl_2$ molten salt activation method ($ZnCl_2$:cotton pulp paper powder = 10 g:1 g), was used to achieve cellulose-derived carbon (CDC) by carbonization (600 °C) for ZIC, owing abundant mesoporous and macroporous structures (Fig. 3(a)) [73], where $ZnCl_2$ can act as the template for pore formation. The CDC assembled aqueous ZIC using a $ZnCl_2$ electrolyte (molar ratio of $ZnCl_2$:$CaCl_2$:H_2O = 1:0.0249:2.583) reached a high capacitance of 357 $F{\cdot}g^{-1}$ at the current density of 0.5 $A{\cdot}g^{-1}$. In addition, the ZIC showed an extremely high capacity of 247 $mAh{\cdot}g^{-1}$ and energy density of 243 $Wh{\cdot}kg^{-1}$ at the power density of 492 $W{\cdot}kg^{-1}$, as well as excellent stability with a capacity retention of 85% after 20,000 cycles.

Porous activated carbon (AC) can be typically obtained from natural resources, e.g., coconut shell [79], accelerating the kinetics of charge transport and providing sufficient active sites for charge storage. AC exhibits its high stability and compatibility with various types of zinc electrolytes. In aqueous $Zn(ClO_4)_2$ electrolyte, it can form hydrogen bonds with H_2O and block the formation of ordered hydrogen bond network, leading to a superior anti-freezing property. Comparing to other electrolytes, $Zn(ClO_4)_2$ electrolyte displayed higher ion conductivity even over a wide temperature

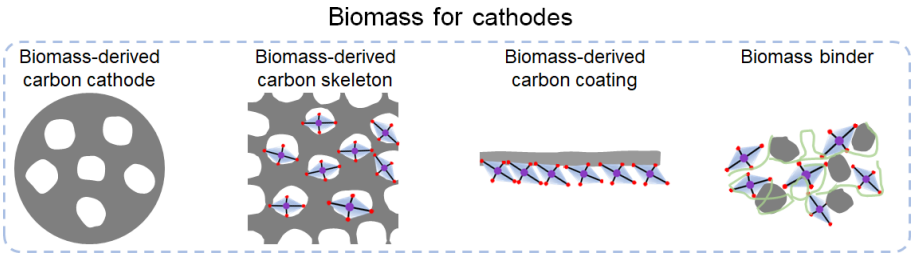

Figure 2 Roles of biomass materials in cathode materials for zinc-based energy storage devices.

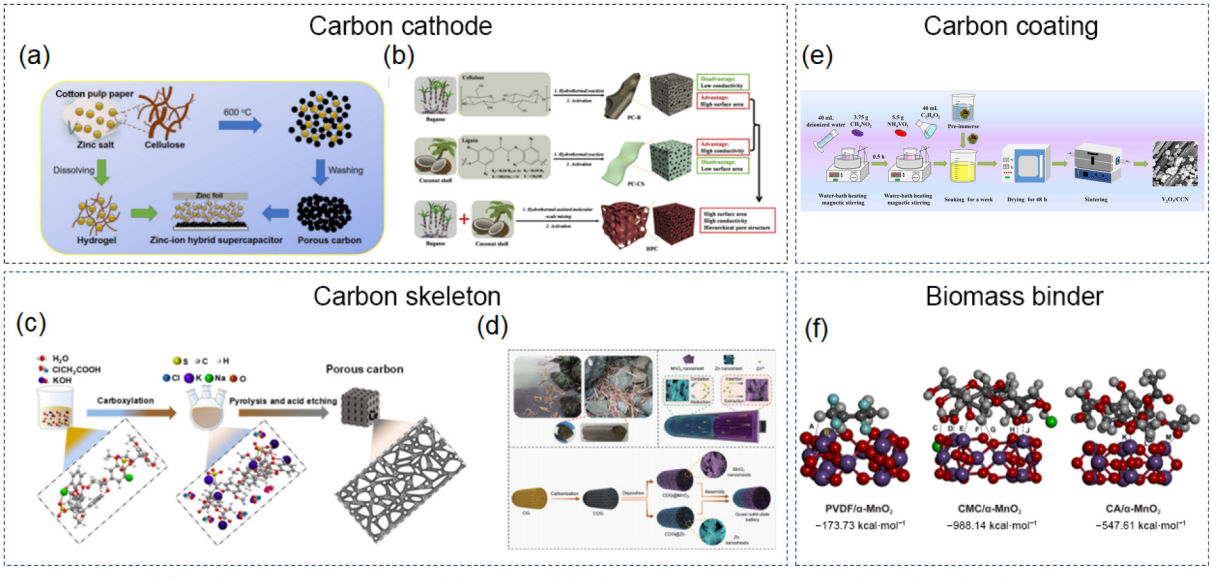

Figure 3 Biomass materials for cathodes in ZESs: (a) Design of the zinc-ion hybrid supercapacitor (ZHS) using cellulose-derived carbon and $ZnCl_2$-contained cellulose hydrogel. Reproduced with permission from Ref. [73], © Elsevier Ltd. 2022. (b) Fabrication of porous carbon from bagasse (PC-B), porous carbon from lignin-rich coconut shell (PC-CS) and HPC. Reproduced with permission from Ref. [74], © Elsevier Ltd. 2019. (c) Schematic illustration for preparation of LHPC-700, LHPC-800 and LHPC-900. Reproduced with permission from Ref. [75], © Elsevier Ltd. 2022. (d) Preparation of the battery component form ocean garbage (OG) and the structure of the carbonized OG (COG)@MnO_2/COG@Zn cell, with its working mechanism. Reproduced with permission from Ref. [76], © The Royal Society of Chemistry 2020. (e) Synthesis of V_2O_3/CCN composites. Reproduced with permission from Ref. [77], © Elsevier Ltd. 2023. (f) Side view of optimized structures and calculated binding energies between a unit cell of α-MnO_2 and the binders: α-MnO_2/PVDF, α-MnO_2/CMC and α-MnO_2/CA. Reproduced with permission from Ref. [78], © American Chemical Society 2021.

range from −50 to 80 °C. Consequently, the ZIC showed an ultrahigh specific capacitance of 423.5 F·g^{-1} and an outstanding high energy density of 190.3 Wh·kg^{-1} at 89.8 W·kg^{-1}. AC derived from coconut shells can be coupled with Zn anode to achieve a high capacitance of 170 F·g^{-1} at a current density of 0.1 A·g^{-1}, with optimizing electrolytes of 1 M zinc triflate ($Zn(OTf)_2$) in acetonitrile [80]. The assembled ZIC possessed good rate performance of ~ 85% capacitance retention at a current density of 2 A·g^{-1}, high energy density of 52.7 Wh·kg^{-1} at 1725 W·kg^{-1} based on the weight of active materials and excellent cycling stability with 91% capacitance retention after 20,000 cycles at a high current rate of 2 A·g^{-1}. A hydrothermal-assisted molecular-scale mixing strategy was proposed to prepare a hierarchical porous carbon (HPC) with a 3D interconnected structure (Fig. 3(b)) [74]. It integrates the advantages of porous carbons from both cellulose-rich bagasse and lignin-rich coconut shell, including high SSA and favorable graphitization degree with good conductivity. The hierarchically porous structure of HPC permits its rapid zinc ion diffusion, extraordinarily efficient electrochemically active surface area and large capacity. In consequence, the ZIC with HPC exhibited an ultrahigh capacity of 305 mAh·g^{-1}, an admirable energy density of 118 Wh·kg^{-1} and an excellent cycling stability of over 94.9% after 20,000 cycles at a high current density of 2 A·g^{-1}. An activated carbon was extracted from corncob (denoted as ACC) as cathode in ZIC, which exhibited superb specific capacitances in acidic, alkaline and neutral electrolytes [81]. By carefully tuning the parameters in calcination–activation process, ACC obtained an ultrahigh SSA of 2619 m^2·g^{-1}, comparing to other carbon materials derived from corncob in literature. The assembled ZIC with 2 M $ZnSO_4$ electrolyte presented a high energy density of 94 Wh·kg^{-1} at 68 W·kg^{-1} in a potential window of 0.2 to 1.8 V and an outstanding cycle stability with only 1.8% capacitance decay after 10,000 cycles at 5 A·g^{-1}. Pencil shaving (PS, mainly including cellulose and lignin) was studied to prepare porous carbon (denoted as PSC-A*x*, where *x* corresponds to KOH-assisted activation temperature) [82]. Through temperature optimization, a well-defined architecture (PSC-A600) was obtained, providing large accessible surface area and numerous active sites for ions adsorption. The as-built PSC-A600/Zn showed a specific capacitance of 413.3 F·g^{-1} at a mass loading of 2.0 mg·cm^{-2} and a high areal capacity of ~ 4.5 F·cm^{-2} even at an ultrahigh loading of 24 mg·cm^{-2}, which lies among the highest performance level ever reported for carbon-based ZICs. The ZIC achieved a high energy density of 147.0 Wh·kg^{-1} at 136.1 W·kg^{-1} and a maximum power density of 15.7 kW·kg^{-1} at 65.4 Wh·kg^{-1} together with outstanding cycling stability, i.e., 61.6% of the initial capacity at 1 A·g^{-1} retained even under a high mass loading of 17 mg·cm^{-2}.

Besides, when applying a unique anti-freezing hydrogel electrolyte of polyacrylamide (PAM) and sodium polyacrylate, the quasi-solid-state hybrid supercapacitor well performed at various bending states and relatively low temperature of −15 °C.

Also, conversion of lignin into hierarchical porous caron is elaborated, owing to its highest natural carbon content. A multi-scale self-template approach was constituted for the preparation of lignin-derived HPCs (LHPCs) with high SSAs (~ 1784 to 2460 $m^2 \cdot g^{-1}$) [75]. Carboxyl groups were introduced into the lignosulfonate (LS) molecules to bond with potassium ions, which increased the active sites in the self-templating process and further transformed into potassium carbonates. Also, the extra potassium chloroacetate could produce KCl. The generated KCl and potassium carbonate can act as multi-scale templating agents, realizing the formation of pore architectures of different sizes. As a result, LHPCs exhibited superb electrochemical performances as electrodes with alkaline and neutral sulfate electrolytes, achieving an ultrahigh energy density of 135 $Wh \cdot kg^{-1}$ at 101 $W \cdot kg^{-1}$. On the other hand, valuable derivatives from lignin are attractive resources for chemical and material synthesis. Furfural, one of the value-added products from lignin fraction, was employed to develop carbon with waxberry-like porous structure, enabling efficient and rapid transport of aqueous zinc ions within the electrode [83]. The assembled ZIC possessed excellent electrochemical performances, including a capacity of 122.3 $mAh \cdot g^{-1}$ at 0.1 $A \cdot g^{-1}$, an energy density of 97.78 $Wh \cdot kg^{-1}$, a power density of 8000 $W \cdot kg^{-1}$ and cycling stability up to 10,000 cycles with capacity retention of 98%. Moreover, the ZIC with 2 M $ZnSO_4$ electrolyte showed a superior low-temperature operability of 78.27 $mAh \cdot g^{-1}$ at −30 °C and stability by three cycles alternating between −20 and 20 °C without performance degradation.

Moreover, biomolecules are investigated, where templates are applied to regulate the microstructure. A protein-rich bone glue was utilized via a templating/activating co-assisted carbonization procedure [84]. The optimized carbon (denoted as BGC) exhibited a highly defect-rich graphitic tissue with hierarchical porous structure, an ultrahigh SSA of 3657.5 $m^2 \cdot g^{-1}$ and an electrochemically active heteroatom doping of 8.0 at.%. Moreover, through comprehensive characterizations and density functional theory (DFT) calculations, the massive heteroatom moieties, i.e., nitrogen (N) and oxygen (O) and lattice defects distributing on BGC surface provide large population of active sites for both Zn^{2+} and OTf^- adsorption, exhibiting capacitive kinetics. As a result, the ZIC employing BGC possessed a maximum capacity of 257 $mAh \cdot g^{-1}$ and retention of 72 $mAh \cdot g^{-1}$ at ultrahigh current density of 100 $A \cdot g^{-1}$, corresponding to 168 $Wh \cdot kg^{-1}$ and 61,700 $W \cdot kg^{-1}$. Two-dimensional (2D) porous N,O co-doped carbon was synthesized via a molten salt method by mixing urea with yeast cell walls in an air atmosphere for ZIC (Fig. 3(c)) [85]. Together with the large SSA, controlled morphology and heteroatom doping, the prepared carbon was optimized by blending with 20 wt.% urea (with resulted doping molar ratio of N:O = 6.03%:9.96%). In the three-electrode system, a surprising capacity retention of 103% was achieved after 10,000 ultralong lifetimes with an energy density of 37 $Wh \cdot kg^{-1}$ at 91 $W \cdot kg^{-1}$.

In short, promising energy and power densities have been achieved in ZICs with biomass-derived carbons (Table 1), which are comparable to their counterparts with other types of advancing carbons with energy densities of ~ 10 to 200 $Wh \cdot kg^{-1}$ and even up to ~ 500 $Wh \cdot kg^{-1}$ and power densities up to ~ 10^5 $W \cdot kg^{-1}$ [86–93]. Besides abundance of natural resources, enriched functional groups and diverse molecular structures can provide biomass-derived carbons with distinct pore structures, promising SSA and network structure and ease of heteroatom doping, which favors charge storage. However, the regulation and homogeneity of the microstructure of biomass-derived carbon is still challenging from the synthetic point of view, where pre-purification or selection could be necessary during processing. Note that ZICs by carbon cathodes and Zn anodes typically present lower energy density and higher power density than ZIBs, with their advantage of cycling stability.

2.2 Biomass-derived carbon as skeleton for cathode materials

As hosts or skeletons for cathodes, biomass materials are acquired

Table 1 Summary of energy densities and power densities of ZICs for the biomass-derived carbons, comparing to their carbon counterparts

Types of carbon materials	Biomass resource	Carbon structure	Energy density ($Wh \cdot kg^{-1}$)	Power density ($W \cdot kg^{-1}$)	References
Biomass-derived carbons	Cotton pulp paper	Porous carbon	243	492	[73]
	Coconut shell	Activated carbon	52.7	1725	[80]
	Coconut shell	Activated carbon	190.3	89.8	[79]
	Corncob	Activated carbon	94	68	[81]
	Pencil shaving	Porous carbon	147	136.1	[82]
	Cellulose	Three-dimensional layer-like carbon	441.7	41,600	[94]
	Lignin	Hierarchical porous carbon	135	101	[75]
	Furfural	Waxberry-like porous carbon	97.78	8000	[83]
	Bone glue	Three-dimensional porous carbon	168	61,700	[84]
	Yeast cell	Two-dimensional nitrogen porous oxygen co-doped carbon	37	91	[85]
Other types of carbons	—	CNTs	~ 10 to 200	~ 100 to 2×10^4	[86, 91]
		Metal-organic framework (MOF)-derived carbon	~ 10 to 500	~ 1–100	[87, 92]
		Porous carbon	~ 10 to 200	~ 1 to 10^5	[90, 93]
		Heteroatom-doped carbons	~ 10 to 100	~ 100 to10^5	[88]
		Hollow carbon spheres	~ 10 to 200	~ 10 to 10^5	[88, 89]

to form pore continuous networks or hierarchical structure. Besides, heteroatom doping can be introduced into the network by adjusting the precursor. By adopting carbon hosts/skeletons, both the kinetics and cycling stability of active materials can be enhanced.

Carbon hosts/skeletons can be typically obtained from fibrous templates, e.g., cellulose nanofibers (CNFs) derived from renewable biomass such as wood, bamboo and agricultural residues, with high aspect ratios and abundant oxygen-containing groups. After freeze-drying and calcination, CNFs could easily form 3D layer-like structured carbon with high SSA, facilitating growth or embedding of targe materials [94]. Also, the 3D networks in CNFs could speed up the transfer of ions/electrons. A unique nickel (Ni)-based composite was obtained by anchoring Ni-NiO nanoparticles onto carbon derived from natural cellulose nanofiber (denoted as Ni-NiO/cellulose nanofiber carbon (CC)), acting as an excellent scaffold with 3D networks for Ni-Zn batteries. Benefiting from the elaborated structure, it can speed up charge transportation and increase the number of active sites of cathode materials, where the capacity of Ni-NiO/CC was remarkably improved from 2.3 to 184 mAh·g^{-1} at 0.625 A·g^{-1}. The as-fabricated Ni-NiO/CC/Zn battery delivered a capacity of 256 mAh·g^{-1} at 0.625 A·g^{-1} with a superior rate performance of 68.5% capacity retention at 25 A·g^{-1} and a good cycling durability of 87.5% retention after 2000 cycles. The Ni-NiO/CC/Zn battery presented a peak energy density of 441.7 Wh·kg^{-1} and a maximum power density 41,600 W·kg^{-1}.

Besides, natural resources are often studied for carbon hosts. Grapefruit peel was adopted to synthesize N-doped carbon carrier powder (CP) through a simple calcination in N_2 atmosphere, where γ-MnO_2 was uniformly electro-deposited onto CP to obtain the composite cathode (γ-MnO_2@CP) [95]. Ascribed to CP, regulation of Mn–O bond distance, Mn valence and Mn domains were achieved, as verified by DFT analysis. The ZIB adopting γ-MnO_2@CP (20 wt.% carbon content) and 3 mol·L^{-1} $ZnSO_4$ electrolyte, delivered a specific capacity of 391.2 mAh·g^{-1} at 0.1 A·g^{-1}, with an outstanding cyclic stability of 92.17% after 3000 cycles at 5 A·g^{-1}. The ZIB showed a remarkable energy density of 553.12 Wh·kg^{-1} together with superior CE of ~ 100%. To further explore the biosafety for the composite cathode, cytotoxicity comparison of pure γ-MnO_2 and γ-MnO_2@CP was carried out, verifying its tremendous potential in clinical medicine application. Reed straw, typical biomass garbage floating on the ocean, is mostly found in wetlands and distributed worldwide, which has a unique nature-designed open porous structure (Fig. 3(d)) [76]. Under high-temperature carbonization, it could be converted into 3D carbon materials with hierarchical pore structures. The honeycomb-like cellular structure with multi-level open channels inside the carbonized reed straw assists the uniform growth of both MnO_2 and Zn nanosheets along the channels. The prepared aqueous MnO_2/Zn battery with 2 M $ZnSO_4$ and 0.1 M $MnSO_4$ exhibited 369.73 mAh·g^{-1} at a low MnO_2 loading of 4.9 mg·cm^{-3} and 306.7 mAh·g^{-1} at a super-high MnO_2 loading of 51 mg·cm^{-3} and an outstanding cycling stability (retention of 95.2% of the initial capacity after 3000 cycles). With poly(vinyl alcohol) (PVA)/LiCl-$ZnCl_2$-$MnSO_4$ gel electrolyte, the as-fabricated quasi-solid-state battery possessed a superior energy density of 20.5 mWh·cm^{-3} (420.1 Wh·kg^{-1}, based on the mass of MnO_2, or 131.5 Wh·kg^{-1} based on the total mass of the battery) among state-of-the-art MnO_2 based ZIBs.

Besides conventional ZIBs, biomass derived carbons can be applied to promote multi-electron charge transfer, as in emerging zinc-sulfur batteries (ZSBs). The problems on S cathode mainly include sulfur dissolution in electrolyte, poor sulfur conductivity (~ 10^{-7} S·cm^{-1}), slow conversion-reaction kinetics, volume expansion during cycling and wettability of aqueous electrolyte on S. Structural design of encapsulating S in conducting carbon hosts presents an efficient manner, e.g., low-cost porous carbon derived from waste jackfruit peel [96], 3D amorphous porous carbon fabricated using coal tar pitch [97]. Note that applying porous carbon host can be further combined with other strategies, like hybrid electrolyte, which facilitates the interfacial wettability with S and eliminates the side reactions on Zn anode. Recently, heteroatom doping has been developed for the biomass-derived carbon host for S cathode. Mangosteen peels were applied, where single cobalt (Co) sites were introduced through Co–CN coordination [98]. Besides obviously increased electric conductivity of S cathode, the enhanced conversion-reaction kinetics was attributed to the high catalytic activity of single-atom Co. Specifically, the single-atom cobalt activates sulfur molecules, reduces the polarization potential between S and Zn.

2.3 Biomass-derived carbon coating for cathodes

Drawbacks of non-carbon cathode materials for ZESs mainly lie in their relatively poor conductivities, dissolution in aqueous environment, volume change or structure collapse during charge/discharge cycling [99]. The above points can be addressed by biomass-derived carbon coatings, which provide ionic conducting tunnels, accommodate volume/structure change and inhibit dissolution of transition metal ions.

Biomass can be integrated into cathode materials during synthesis. Carbon-coated V_2O_5 microspheres were designed by a hydrothermal route with the introduction of chitosan, leading to the formation of nanosheets with an interconnected porous structure [100]. It provides sufficient internal tunnels to buffer the volume changes during cycling, thus efficiently enhancing the electrical conductivity of active materials. The SSA of V_2O_5 coated by 0.25 g chitosan (noted as V_2O_5@0.25 C) significantly increased comparing to that of the pristine V_2O_5, which is conducive to the wide distribution of active sites, thereby improving the storage capacity of zinc ions. Therefore, the as-assembled V_2O_5@0.25 C/Zn cell achieved an exceptional specific capacity of 532.4 mAh·g^{-1} at 0.2 A·g^{-1} with an energy density of 354.9 Wh·kg^{-1} and showed long-term cycling stability with a retention rate of 86% after 3000 cycles at 5 A·g^{-1}. The V_2O_3/carbonized chestnut needle (V_2O_3/CCN) composites were successfully prepared by a simple evaporation-induced self-assembly technique, using NH_4VO_3 and chestnut needle as raw materials (Fig. 3(e)) [77]. Chestnut needle decomposed and volatilized, forming a unique porous structure to provide a three-dimensional conductive framework for V_2O_3, which facilitates the rapid transport of electrons and Zn^{2+} and effectively inhibits the dissolution of vanadium. The prepared V_2O_3@CCN cathode maintained a rod-like array structure with numerous pores, which can enhance the contact area between the electrolyte and the cathode and offer additional active sites. By galvanostatic intermittent titration technique (GITT), the diffusion coefficient of V_2O_3@CCN was determined to be between $10^{-10.5}$ and $10^{-8.5}$ cm^2·s^{-1}, much higher than other carbon composites for V_2O_3. Benefiting from the above-mentioned features, V_2O_3/CCN-15/2 (weight ratio ($W_{NH_4VO_3}$:$W_{chestnut\ needle}$) = 15:2) possessed a high discharge capacity of 431.96 mAh·g^{-1} at 0.05 A·g^{-1} and a fabulous

cycle capability of 201.41 mAh·g^{-1} (capacity retention of 94.27%) at 3 A·g^{-1} after 1000 cycles. *Ex situ* study revealed that the structure of V_2O_3 transformed to VO_2, whose crystalline structure underwent reversible change during charge/discharge. Glucose-derived carbon was incorporated into LiVO (LiVO/C-glucose (G)) for aqueous ZIB [101]. The introduction of carbon coating can not only augment the electrical conductivity of the LiVO matrix, but also reduce the interaction between Zn^{2+} and the LiVO framework, facilitating the diffusion of Zn^{2+}, as verified by DFT calculations. LiVO/C-G underwent dual phase transitions during charge/discharge cycles, resulting in an amorphous vanadium oxide derivative for subsequent electrochemical reactions. And the assembled ZIB delivered a capacity of 145.9 mAh·g^{-1} at 1 A·g^{-1} and maintained a capacity retention of 95.5% over 1000 cycles.

Post-synthesis methods are also developed to mix biomass-derived carbon and cathode materials. A long sonication process was designed by using pitaya peels-derived carbons and Nb_2C MXenes to obtain the well mixed Nb_2C-PCarbons CPs [102]. The derived low-cost porous carbon with heteroatom O doping owns the advantages of high SSA, extensive doped-atoms produced-defects, raised active sites and regulated conductivity. When applied as cathode in ZIB, it showed an excellent energy storage capability of 239.7 mAh·g^{-1} at 0.1 A·g^{-1}. And even at 10 A·g^{-1}, the cell still harbored a brilliant rate performance about 54.3 mAh·g^{-1}.

2.4 Biomass as binder for cathodes

Moreover, biomass materials with aqueous compatibility and abundant functional groups can be promising candidates for cathode binders, where the interaction between the binders and cathodes may play an important role. The approach of green binder demonstrates its great potential of endowing the process with reducing cost and increasing sustainability.

The effects of green binders for cathodes, i.e., sodium carboxymethyl cellulose (CMC) and cellulose acetate (CA), were compared with that of the conventional polyvinylidene fluoride (PVDF) for ZIBs (Fig. 3(f)) [78]. CMC and CA binders have the carboxylic (–COOH) and hydroxide (–OH) groups that can preferentially form strong H-bond with oxygen in α-MnO_2, stabilizing the integrity of components in cathode (Fig. 3(f)). Meanwhile, Na^+ in the anionic CMC structure has additional abilities to pull in and maintain Zn^{2+} concentration close to active materials. The CMC-based ZIB was able to maintain high ionic diffusivity by GITT analysis. Also, the interaction between binders and α-MnO_2 was investigated via DFT to affirm the high stability of the ZIB/α-MnO_2 with the CMC binder.

When biomass is converted into advancing carbon nanostructures as cathodes or integrated into cathodes as skeletons, the tuning of microstructure characteristics as well as homogeneity acquires further elaboration. The derived carbons can be further utilized as coatings for cathodes, influencing the reaction kinetics, where the introduction of active sites might be a potential solution to boost performance. Also, it favors the stability of cathode materials by depressing the dissolution of transition metal ions and providing room for volume change. Besides, green binders are being investigated for novel processing in rechargeable batteries due to their affinity to the transition metal ions, where their stability as well as rheological properties warrants further study.

3 Biomass materials for zinc electrolytes

When involved in electrolytes (Table 2), hydrophilic functional groups in biomass, such as –OH, –COOH, –NH_2, –CONH– and –$CONH_2$, have high adsorption affinities for polar solvent molecules, like water (Fig. 4). The strong interaction between Zn^{2+} and these functional groups can change the zinc solvation structure and charge transport behavior. Further, it can guide the interfacial ion transport, promoting the uniform distribution of Zn^{2+} on Zn surface and hence induce homogeneous Zn deposition and depress Zn dendrite growth. Also, biopolymers can be easily processed into customized shapes as in gel or quasi/solid-state electrolytes, with the advantages of wide EW, (~ 1.8 to 3.9 V vs. Zn/Zn^{2+}), high ion conductivity (~ 5.4 to 82 mS·cm^{-1}), flexibility, anti-frozen ability, biocompatibility and mechanical properties (excellent elasticity, self-healing ability and high adhesion). By adopting biomass in

Table 2 Physicochemical properties of the biomass-incorporated zinc electrolytes

Zinc salt	Concentration	Matrix	EW (oxygen evolution reaction (OER), V vs. Zn/Zn^{2+})/HER	Ion conductivity (mS·cm^{-1})	DOD (%)	References
$ZnSO_4$	2 M	CMC	—	20.7	2.12	[103]
$ZnCl_2$	$ZnCl_2$:H_2O = 1:2.2 (DES)	Cellulose	3.9/–0.59	5.4	85	[104]
$ZnSO_4$-$MnSO_4$	2 M + 0.1 M	Xanthan gum 20 wt.%	2.2; –0.2–2	16.5	—	[120]
$ZnSO_4$-$MnSO_4$	10 M + 1 M	Cellulose-TEOS	—	32.3@20 °C	1.36	[106]
$ZnSO_4$-$MnSO_4$	2 M + 0.1 M	GG	—	10.7	—	[121]
$ZnSO_4$-Li_2SO_4	0.5 M + 0.5 M	Gelatin	—	6.15	3.4	[122]
$ZnSO_4$-$MnSO_4$	2 M + 0.1 M	SA	2.7; –0.2–2.5/–0.2	—	4.08	[115]
$ZnSO_4$-$MnSO_4$	1 M + 0.2 M	PAM-alginate-SA	—	29.2	—	[117]
$ZnSO_4$	0.41 M	CMC	—	—	—	[107]
$ZnSO_4$	1 M	Gelatin	—	—	—	[150]
$ZnSO_4$	1 M	GG	—	—	—	[112]
$ZnSO_4$-$MnSO_4$	2 M + 0.2 M	SA	—	18.3	—	[109]
$ZnSO_4$-$MnSO_4$	2 M + 0.1 M	PVA-gelatin-cellulose-α	—	12.3	—	[126]
$ZnSO_4$-$MnSO_4$	1 M + 0.1 M	HPE acryl amide N,N'-methylenebisacrylamide	—	17.6	—	[123]

(Continued)

Zinc salt	Concentration	Matrix	EW (oxygen evolution reaction (OER), V vs. Zn/Zn^{2+})/HER	Ion conductivity ($mS·cm^{-1}$)	DOD (%)	References
$ZnSO_4$-$MnSO_4$	2 M + 0.1 M	GG-SA	2.31@GG/SA	25.37@GG/SA	—	[125]
$ZnSO_4$	2 M	TA-SA	—	24.2	—	[111]
$ZnSO_4$-$MnSO_4$	2 M + 0.2 M	Alginate	—	25	—	[110]
$ZnSO_4$	2 M	Lignin-chitosan	2.65; −0.25–2.4	18.6	—	[119]
$ZnSO_4$	2 M	Gelatin	2.68	23.5	—	[113]
$ZnCl_2$	$ZnCl_2$:H_2O = 1:4.3	Cellulose	1.8; 0–1.8	74.9	—	[116]
$ZnCl_2$-$CaCl_2$	$ZnCl_2$:$CaCl_2$:H_2O = 1:0.26:2.8	Cellulose	—	74.9	—	[108]
$ZnCl_2$	10 M	PVA-gelatin	2.31; 0.26–2.57	20.8	—	[114]
$Zn(OAc)_2$ (OAc refers to acetate)	0.2 M	PAM-SA	—/−0.025	82	—	[118]
$ZnSO_4$		Gelatin	2.75; −0.25–2.5	—	—	[124]

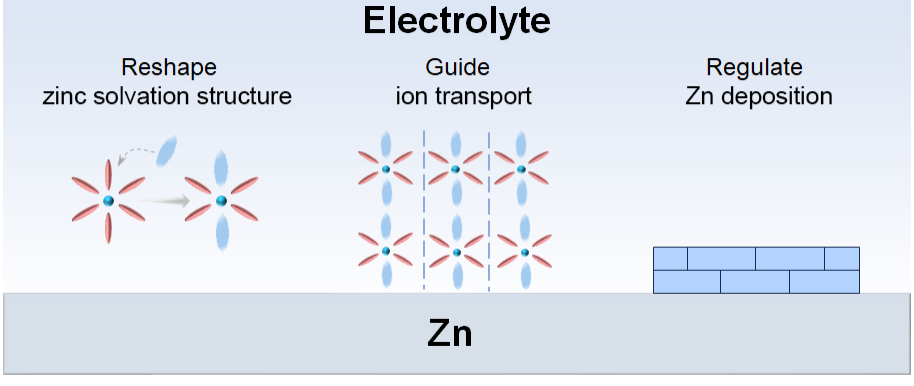

Figure 4 Roles of biomass materials in zinc electrolytes for ZIBs.

electrolytes, stable Zn stripping/plating can be widely achieved, with a depth of discharge (DOD) ~ 1.36% to 85%.

3.1 Additives in liquid electrolyte

When applied in aqueous electrolytes, the concentration of incorporated biomass materials is one fundamental factor for the electrolyte properties. The dispersion concentration of biopolymer could be very low in an aqueous solution, which however can be comparable to that of water if DES can form.

CMC was proposed as an additive in $ZnSO_4$, simultaneously tailoring the solvation structure, hydrodynamic stability and Zn deposition behavior (Fig. 5(a)) [103]. Being water-dispersible, CMC is typically applied as binder for cathode in aqueous battery. Possessing abundant $–COO^-$ and –CO– groups, CMC additive interacts with Zn^{2+}, which alters the solvation structure and constrains water activity. Through nuclear magnetic resonance (NMR) spectrum, confined D_2O water molecules were partially freed, suggesting that the water molecule in solvation sheath is replaced by $–OCH_2COO^-$ groups. As a result, water-induced side reactions including HER reaction, Zn corrosion and passivation, could be suppressed. Through *in situ* optical microscope, the delayed hydrodynamic instability was verified by no protrusions during Zn plating. When applied in $ZnSO_4$, the added CMC led to the growth of Zn (101) after stripping/plating as confirmed by X-ray diffraction (XRD). DFT calculations reveal that CMC is inclined to adsorb onto the (101) facet of Zn with lower adsorption energy compared with that on (002) (Fig. 5(b)). Finite element simulation showed that with CMC, the deposited Zn demonstrates a greater tendency to fuse at the nucleation sites, leading to the anisotropic growth of (101)-dominated texture.

Considering that DESs are long applied in biomass dissolution, biomass molecules are elaborated as DES components. A cellulose-complexing strategy was proposed to develop $ZnCl_2$-based DES, i.e., $ZnCl_2$-cellulose electrolytes (ZCEs, $ZnCl_2$:nH_2O, with n = 2.2), which is able to reconstruct Zn^{2+} coordination, tune water activity and regulate solid-electrolyte interface (Fig. 5(c)) [104]. Deconvolution of Fourier transform infrared (FTIR) spectra and DFT calculations reveal that glucose unit can participate into the solvation shell of Zn^{2+} when n is below 3, meanwhile forming H-bond network with the released water molecules. It then led to the widened EW (from 3.3 to 3.9 V vs. Zn/Zn^{2+}) and depressed water-associated side reactions. Through *ex situ* characterization, an organic-dominant composite layer with Zn^{2+}-cellulose complex was discovered. At the same time, an increased intensity for Zn (002) texture induced dendrite-free Zn deposition. Thus, ZCEs could lead a DOD of 85% at 50 $mA·cm^{-2}$ and 50 $mAh·cm^{-2}$, which is among the highest records in novel electrolytes.

3.2 Components for gel electrolyte

A wide classes of biomass have been applied to gel electrolytes, including polysaccharides, polyphenols, proteins and their combinations (Fig. 6), where their applications in a wider scope of

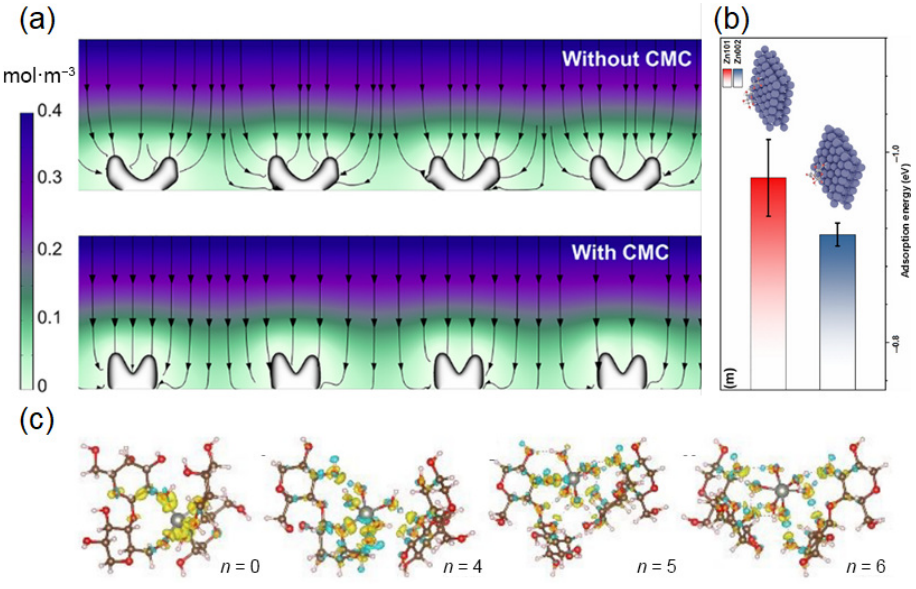

Figure 5 Biomass as additives in zinc electrolytes: (a) finite element method (FEM) simulation of the growth of nucleation sites by CMC-containing electrolyte and (b) adsorption energies for CMC on different Zn facets. Reproduced with permission from Ref. [103], © Elsevier B.V. 2023. (c) Charge density difference maps for coordination of cellulose to $[Zn(OH_2)_n]^{2+}$ in clusters $[Zn(OH_2)_n]^{2+}$·2cellulose. Reproduced with permission from Ref. [104], © The Royal Society of Chemistry 2023.

energy storage devices can be referred to the well-formalized recent reviews [105]. The following discussion is sorted according to the types of biomass-based gel electrolytes in ZESs.

Polysaccharide. By using cellulose-rich cotton as raw material, tetraethyl orthosilicate as crosslinker and glycerol as anti-freezing agent, a facile and cost-effective method was developed to construct an all-round hydrogel electrolyte (CT*y*G30, where C, T, *y*, G and 30 represent cellulose, tetraethylorthosilicate (TEOS), the milliliters of TEOS added, glycerol and the milliliters of glycerol added, respectively) (Fig. 6(a)) [106]. The CT*y*G30 gel possessed high ionic conductivity, excellent mechanical properties, ultralow freezing point, good self-healing ability, high adhesion and good heat-resistance ability. Through thermal analysis, CT3G30 displayed a high tolerance to low- and high-temperature working environments, owing to the good thermal stability of both cellulose and siloxane linkages and anti-freezing property of glycerol. It possessed a high ionic conductivity of 32.3 mS·cm^{-1} at 20 °C and even afforded 19.4 mS·cm^{-1} at −40 °C. Benefiting from appropriate crosslinking, the excellent adherence of CT3G30 guarantees close contact with Zn. Meanwhile, the electrostatic interaction between CT3G30 framework and Zn^{2+} ions confines the 2D diffusion of Zn^{2+}, homogenizing Zn deposition. High-voltage coaxial-fiber aqueous rechargeable ZIBs (CARZIBs) were designed by adopting Zn nanosheet arrays (NSAs) on carbon nanotube fiber (CNTF) as the core electrode and ZnHCF composite on aligned CNT sheets (ACNTSs) as the outer electrode, with $ZnSO_4$-CMC as the gel electrolyte (Fig. 6(b)) [107]. CARZIBs not only enabled aligned charge transport path, large SSA and small contact resistance of the coaxial structure, but also provided superior mechanical flexibility and stability after long-term bending. Zn NSAs were homogeneously and densely electrodeposited on CNTF surface. After bending 3000 times, the CARZIBs still retained 93.2% of its initial capacity, indicating remarkable wearability. A flexible zinc ion hybrid supercapacitor was constructed by a solid-state cellulose hydrogel electrolyte containing high concentrated of $ZnCl_2$ ($ZnCl_2$:H_2O = 1.75 g:1 g), affording a wide EW, an excellent ionic conductivity of 74.9 mS·cm^{-1} [116]. Due to the extremely low content of water bonded with Zn^{2+}, the formation of irreversible by-products by side reactions on Zn was restricted. Also, a high concentration of Zn^{2+} in cellulose hydrogel contributed to a low concentration gradient on Zn surface, restricting Zn dendrite growth. Moreover, the hybrid supercapacitor with cellulose hydrogel electrolyte possessed a low temperature tolerance at −20 °C considering its cycling stability. Cotton cellulose was dissolved by a specially designed $ZnCl_2/CaCl_2$ ($ZnCl_2$:$CaCl_2$:H_2O = 9.87 g:0.2 g:3.63 g) solution to form a hydrogel [70]. Besides a high ion conductivity of 74.9 mS·cm^{-1}, the hydrogel presented excellent freeze-tolerance as low as −70 °C, self-healing, remoldability, reusability and superior thermal reversibility. The remoldability could be attributed to the thermally induced transformation (Fig. 6(c)) and the 3D-printable feature could be viewed by dynamic shear moduli measurement.

A cathode-stabilized hydrogel electrolyte (CSHE) from SA was prepared [117]. And covalent crosslinking PAM was further incorporated into CSHE to enhance the polymetric framework and form a robust 3D porous structure for hybrid hydrogel electrolyte. SA-PAM displayed an excellent ionic conductivity of 29.2 mS·cm^{-1} and high resistance to binding, twisting and cutting. SA-PAM was then coupled with a sodium pre-intercalated cathode δ-$Na_{0.65}Mn_2O_4$·1.31H_2O, forming a robust and flexible ZIB. Compared with 70.1% capacity retention for the cell with pristine SA, the full cell with SA-PAM exhibited a superior capacity retention of 96% over 1000 cycles at the current of 2 A·g^{-1}. Ecofriendly solid-state electrolyte (hierarchically three-dimensional Zn^{2+}-conductor gel electrolyte (Alg-Zn)) was designed based on the ion-crosslinking between carboxylate groups of alginate and Zn^{2+} ions, possessing ion confinement, tremendous long shelf life and outstanding restoration ability (Fig. 6(d)) [109]. Owing to the ion confinement effect of carboxylate groups in Alg-Zn, ion transport and self-diffusion can be greatly restricted, suppressing dendrite growth and formation of irreversible by-products. A green and programmable electro-crosslinking strategy was proposed, to *in situ* prepare a multi-layer hierarchical Zn-alginate polymer electrolyte (Zn-Alg) via the superionic binds between the carboxylate groups

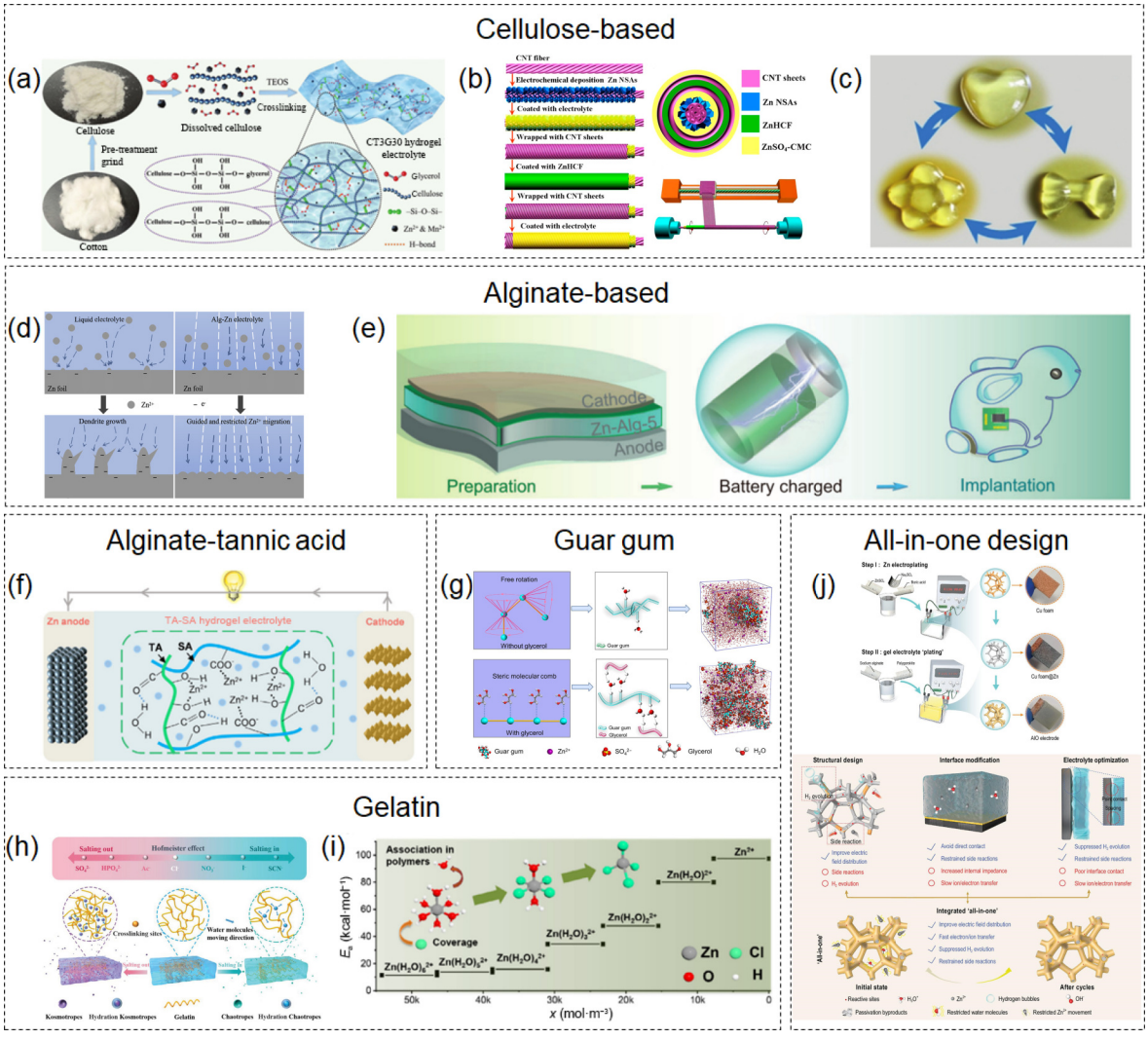

Figure 6 Biomass in gel electrolytes: (a) Synthesis of CT3G30 hydrogel electrolyte. Reproduced with permission from Ref. [106], © Wiley-VCH GmbH 2021. (b) Fabrication of CARZIB. Reproduced with permission from Ref. [107], © American Chemical Society 2019. (c) The remoldability of gel–glycerol. Reproduced with permission from Ref. [108], © Wiley-VCH Verlag GmbH & Co. KGaA, Weinheim 2019. (d) Deposition behaviors of Zn^{2+} in $ZnSO_4$ + $MnSO_4$ aqueous electrolyte and Alg-Zn electrolyte. Reproduced with permission from Ref. [109], © Elsevier B.V. 2020. (e) Schematic diagram of biocompatible applications using rabbit models. Reproduced with permission from Ref. [110], © Xie, X. S. et al. 2022. (f) Schematic illustration of the fabrication of TA-SA hydrogel electrolyte. Reproduced with permission from Ref. [111], © Science China Press 2022. (g) Steric molecular combing effect for GG molecular conformation regulation. Reproduced with permission from Ref. [112], © American Chemical Society 2022. (h) Hofmeister effect. Reproduced with permission from Ref. [113], © Wiley-VCH GmbH 2023. (i) The change of E_a in the desolvation process of $[Zn(H_2O)_6]^{2+}$ in the PVA-gelatin hydrogel-based HiSE. Reproduced with permission from Ref. [114], © Elsevier B.V. 2022. (j) Schematics of structural design, interface modification, electrolyte optimization and integrated "all-in-one" system. Reproduced with permission from Ref. [115], © Li, C. P. 2021.

and Zn^{2+}, achieving a high ionic conductivity of 25 mS·cm^{-1} (Fig. 6(e)) [110]. Zn-Alg afforded highly reversible Zn plating/stripping at 5 mA·cm^{-2} and 1.25 mAh·cm^{-2}. Through conducting rabbit models, the battery with Zn-Alg was bio-compatible and safe. Moreover, biomass-based hydrogel can be successfully applied to other types of ZESs. For instance, a dual-network structured hydrogel electrolyte composing of PAM and SA and potassium iodide was developed for solid-state zinc-air/iodide hybrid batteries, with excellent water retention capacity and regulated Zn^{2+} solvation structure [118]. Based on Raman spectra, iodide ions in the hydrogel reshapes the solvation structure of zinc ions, meanwhile strengthening the –OH bond in H_2O and depressing the reactivity of H_2O.

Polyphenols. A simple yet effective scalable fabrication of free-standing gel polymer electrolytes was reported, consisting of chitosan and LS (LS-chitosan) or micellar dispersion of lignosulfonate with softwood kraft lignin (LSKL-chitosan) [119]. The formulation combines the renewability, low cost and thermomechanical resistance. The improved thermal stability indicates that LSKL-chitosan and LS-chitosan gel polymer electrolytes (GPEs) are appealing to physically isolated battery electrodes at high temperatures, avoiding the risk for short-circuit upon thermal runaway.

A cross-linked composite hydrogel consisting of TA and SA was prepared, enhancing ion-confined properties, changing Zn^{2+} solvation structure and providing a high ion conductivity of 24.2 mS·cm^{-1} and mechanical strength (Fig. 6(f)) [111]. Via FTIR spectra, Zn^{2+} could crosslink with the negatively charged –COO groups in SA and chelate with –OH in TA. Consequently, the activity of water in the Zn^{2+} solvation sheath decreased and the

water-based parasitic side reactions were mitigated. Comparing to the one with SA, the gel electrolyte with TA-SA could guide more uniform Zn deposition to achieve steady Zn stripping/plating.

Proteins. A stable bio-electrolyte was fabricated by readily mixing a high-salt-tolerant, water-soluble xanthan gum with aqueous sulfate solution [120]. Besides its excellent mechanical properties, the gel was hydrating, adhesive and adaptive, which slowed down the corrosion of Zn and suppressed the growth of Zn dendrite. GG biopolymer electrolyte possessed remarkable flexibility and a wide temperature working window (5–45 °C) [121]. Besides excellent kinetics in Zn|Zn cell with GG electrolyte, the quasi-solid-state ZIB with GG electrolyte exhibited remarkable rate performance showing discharge capacities of 279.4, 227.9 and 181.6 mAh·g^{-1} recorded at current densities of 0.6, 1.5 and 3.0 A·g^{-1}, respectively. Also, it presented excellent flexibility after bending tests, demonstrating its promising potential in personalized wearable devices. A highly stable quasi-solid-state ZIB with glycerol into the GG electrolyte was constructed, possessing an ultrafast self-healing ability and low solvation coordination characteristics to realize a robust interphase towards dendrite-free Zn anode (Fig. 6(g)) [112]. With the addition of glycerol, it could comb better and straighten molecular chains and inhibit intramolecular rotation, so that the resultant exposed alcoholic hydroxyl active sites could be dynamically crosslinked with borate to achieve an ultrafast self-healing capability of ~ 0.5 min comparing to ~ 10–1400 min for the literature values. In addition, the gel electrolyte had a strong binding energy with active water molecules, which could change the H_2O coordination number in the solvation shell from 6 to 3.8. Thus, a continuous and uniform ion transport channel was formed. Meanwhile, due to ultrafast self-healing characteristics, stable Zn stripping/plating could be achieved for more than 400 h at 10 mA·cm^{-2} and 10 mAh·cm^{-2}.

A durable, self-standing and flexible gelatin hydrogel electrolyte (GHE) for rechargeable solid-state ZIB was prepared, with a high ionic conductivity, robust mechanical strength and intimate contact with electrodes [122]. Attributable to the considerable porosity of gelatin hydrogels and thereby high aqueous electrolyte reservation capability, GHEs exhibited high ionic conductivities. Due to homogenous contact between GHEs and Zn foil, an even ion transport and regulated Zn plating with a small deposition current was guaranteed. A novel hierarchical gelatin and PAM based hierarchical polymer electrolyte (HPE) electrolyte was prepared with favorable mechanical strength and safety [123]. The high conductivity of HPE of 17.6 mS·cm^{-1} could be attributed to its high water-holding capacity and highly porous 3D structure. The developed flexible and wearable solid-state ZIB possessed impressive safety performance, including working under a variety of severe conditions, such as being bent, hammered, punctured, cut, sewed and washed in water and put on fire. Based on the "salting out" phenomenon in Hofmeister effect, a gelatin-based hydrogel electrolyte (GGE) membrane was fabricated, possessing a high ionic conductivity of 23.5 mS·cm^{-1} (Fig. 6(h)) [113]. Kosmotropic salt ions on the left side of the Hofmeister sequence have weak interaction with hydrophilic polymer chains but strong solvation with water molecule. This could weaken the interaction between hydrophilic polymer chains and aqueous solution, thereby reducing the solubility of polymer in aqueous solution, leading to "salting out". The "salting out" phenomenon strengthens the H-bond and hydrophobic effect of polymer chain segments, resulting in more entanglement and binding of polymer chain segments, thus improving the strength of polymer hydrogels and increasing their flexibility and toughness. An eco-friendly Zn ion hybrid battery was fabricated using a PVA-gelatin hydrogel-based water-in-salt electrolyte (HiSE), where the HiSE presented a high ionic conductivity of 20.8 mS·cm^{-1} and adjustable mechanical properties [114]. When water molecules in the hydrated zinc ions are snatched away, chlorine ion rapidly replaces to form $[Zn(H_2O)_{6-x}Cl_x]_{2-x}$, leading to the lower activation energy (E_a) in the desolvation process of $[Zn(H_2O)_6]^{2+}$ (Fig. 6(i)). The water-deficient solvation structure in HiSE can enhance water retention capacity and eliminate the deterioration of electrochemical performance by rapid water loss as in conventional hydrogels. A dynamically healable hydrogel electrolyte was designed with a highly reversible solgel transition, which could construct a conformal electrode–electrolyte interface and further evolve into a stable solid–solid interphase by *in situ* solidification [124]. Ascribed to the confinement of water molecule as verified by FTIR, EW of GGE was significantly expanded to ~ 2.75 V with decreasing active water content. As verified by DFT, uniform Zn^{2+} migration channels formed between the helical gelatin chains in the GGE through the bridge effect of sulfate groups due to strong interaction between SO_4^{2-}, the hydroxyl group and the amide on the gelatin chain, which can guide the homogeneous Zn deposition.

Combinations. By mixing GG, SA and ethylene glycol (EG), a composite GG/SA/EG hydrogel electrolyte was developed with high ionic conductivities (25.37 mS·cm^{-1} for GG/SA; 16.81 mS·cm^{-1} for GG/SA/EG), excellent mechanical properties and anti-freezing characteristics [125]. When stored in −20 °C for 2 h, GG/SA/EG hydrogel well retained its hydrogel state and mechanical properties, exhibiting high elasticity to sustain various large deformation of twisting. On the other hand, GG and GG/SA hydrogels were broken under large twisting. By using cellulose aerogel-gelatin (CAG) solid state electrolyte, an implantable and rechargeable transient battery was fabricated with excellent biocompatibility and complete degradability [126]. Possessing a highly porous 3D structure and liquid storage capacity, CAG owned an ultrahigh ionic conductivity at room temperature. By introducing CAG solid electrolyte and a plasticized silk fibroin package pocket, the flexibility and mechanical stability could be improved. The fabricated battery could be almost completely degraded with 30 days both *in vitro* and *in vivo*, where the substances produced during the degradation process were non-toxic and harmless. Biopolymers can be also integrated with synthetic polymers, like SA-polyacrylamide [127].

An "all-in-one" (AIO) electrode was designed by combining the strategies of structural design (3D skeleton), interface modification (sufficient interface contact) and electrolyte optimization (mixed gel electrolyte) (Fig. 6(j)) [115]. This AIO design can increase the electrode/gel electrolyte contact area and improve electrode adaptability of volume change. The gel electrolyte was tightly integrated with the electrode, providing channels and active sites for ion transportation and redox reactions. In addition, as most water molecules in the gel electrolyte were constrained, HER and side reactions induced by active water were greatly suppressed.

Biopolymers can function as additives or hosts in the electrolytes for ZESs, owning advantageous electrochemical windows and ionic conductivities as in Table 2. Also, they possess great potential to be combined with other classes of materials as quasi-solid-state electrolytes. Note that controlling the content of solvent amount, like water molecules, in the electrolyte systems, can be critical when

tuning its physicochemical properties [128]. Also, advancing design of gel electrolyte can further address the interfacial compatibility between electrolyte and electrode [129–131]. Besides, the functionalities of biomass-based electrolytes will be further exploited in aqueous batteries, towards mechanical and low-temperature tolerance.

4 Biomass materials for separators/membranes

Biomass can be directly applied in membranes, which can crosslink with the electrolyte and form hydrogen bonds with H_2O, thus depressing water activity and inhibiting water-induced side reactions, regulating charge transport behavior and inducing surface structure formation.

Direct coating of biopolymer is efficient to functionalize separator. By coating chitosan on the conventional filter paper separators, it suppressed proton activity and changed ion transport behavior (Fig. 7(a)) [132]. The hydroxyl, amino and ether groups on chitosan allow preferential adsorptions of proton, Zn^{2+} and sulfate, which suppress the proton activity and inhibit the corrosions and HER on Zn. In addition, the interactions of Zn^{2+} and sulfate with chitosan regulate the ion transport manner and enlarged Zn^{2+} transference number, which ensure the homogeneous Zn nucleation and growth. With the application of chitosan-filter paper separators, stable Zn plating/stripping was realized for 450 h at 5 mA·cm^{-2}, 1 mAh·cm^{-2}, with CEs reaching 99.6%.

Cotton-derived cellulose film (CF) was employed by a facile filtration method as the separator for ZIBs, which is an inexpensive large-scale manufacturing technique (Fig. 7(b)) [133]. Originating from abundant surface hydroxyl groups in the cellulose, the contact angle of ~ 0° demonstrated the excellent electrolyte affinity. The CF separator offered dense and uniform nanopores, excellent mechanical properties of 29.2 MPa in strength and 4.16 GPa in modulus and a large ionic conductivity of 56.95 mS·cm^{-1}. Meanwhile, the Zn^{2+} transference number greatly increased from 0.29 to 0.48, contributing to alleviating the concentration gradient on the interface. E_a with the CF separator was estimated to be 33.6 kJ·mol^{-1}, lower than that with the glass fiber (GF) separator (43.4 kJ·mol^{-1}). It indicates that the CF separator can facilitate desolvation and enhance interfacial kinetics. In addition, Zn nucleation overpotential was reduced from 70.1 to 48.3 mV, suggesting the promoted uniform Zn plating as verified by atomic force microscope (AFM) images (Fig. 7(c)). A nature-inspired separator (BC/ZnHAP) was developed via the hybridization of the biomass-derived bacterial cellulose (BC) network and nano-hydroxyapatite particles (HAP) [135]. BC/ZnHAP can not only suppress the water activity and alleviate the water-induced side-reactions, but also boost ion transport kinetics and homogenize Zn^{2+} flux. Remarkably, the Zn|Zn symmetric cell with BC/ZnHAP harvested a stable cycling over 1025 h and 611 h even at a high DOD of 50% and 80%, respectively. The V_2O_5/Zn full cell with a low negative/positive (N/P) capacity ratio of 2.7 achieved a superior capacity retention of 82% after 2500 cycles at 10 A·g^{-1}. Furthermore, the ZnHAP separator could be totally biodegraded within 2 weeks.

Compositing is another general approach to incorporate biomass into membrane. To achieve better performance and reduce the cost, composite Nafion membranes were synthesized by introducing biomass waste, lignin (Fig. 7(d)) [134]. With the addition of lignin, the ion conductivity increased to 9.1 × 10^{-2} mS·cm^{-1}. Rich –OH groups in lignin favor the enrichment of proton/cation channels. With the composite membrane, the growth of lateral zinc hydroxide sulphate parallel to the surface was promoted.

An innovative solution was proposed by introducing an ultrathin (~ 2 μm) unprocessed reed membrane as an intimate artificial interphase [136]. Leveraging the advantages of abundant –OH groups, nanoscale ion regulation tunnels and excellent mechanical properties, the reed membrane facilitated uniform Zn^{2+} flow, promoted the desolvation of hydrated zinc ions and effectively suppressed dendrite penetration. Furthermore, the formation of Zn–O bonds resulted in a protective layer covering Zn surface during cycling. Consequently, the symmetric cell with the membrane exhibited remarkably reversible depositing/stripping

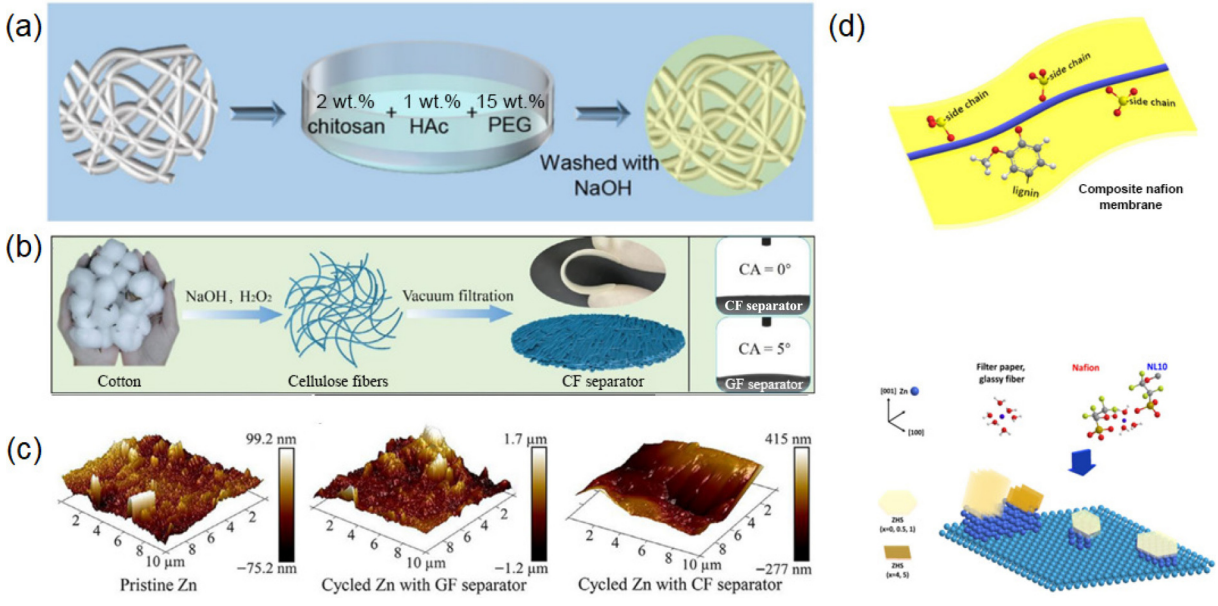

Figure 7 Biomass for membrane/separators: (a) Preparation of CS-filter paper. Reproduced with permission from Ref. [132], © Elsevier B.V. 2022. (b) Fabrication of CF separator. (c) AFM images of the pristine Zn electrode, with the GF separator and with the CF separator. Reproduced with permission from Ref. [133], © Elsevier B.V. 2021. (d) Design of composite biomass waste lignin@Nafion membranes and proposed scheme to summarize the effects of membranes on the surface of Zn metal. Reproduced with permission from Ref. [134], © Wiley-VCH Verlag GmbH & Co. KGaA, Weinheim 2019.

over 1450 h at 3 mA·cm^{-2} and 1.5 mAh·cm^{-2}. Simultaneously, the Cu|Zn half cell demonstrated outstanding average CE, exceeding 99.77% throughout 3000 cycles. Also, the assembled AC/Zn ZIC manifested an exceptional cyclic stability with a capacity retention rate of 88.95% after undergoing 4000 cycles.

Besides the above functions, the use of biopolymers in separators/membranes can bring the merit of cost effectiveness. Meanwhile, the processing need to be compatible with their polymeric nature, which might limit the choices of solvents but trigger the application of DESs. Also, the mechanical properties of membranes/separators could be further improved due to low modulus of biopolymer, where composite with inorganic materials might serve as an efficient manner.

5 Biomass materials-based surface layer for Zn anode

An artificial SEI physically inhibits the direct contact between electrode and electrolyte and slows down the occurrence of side reactions including HER and passive corrosion, to improve the utilization of Zn (Fig. 8). Due to the strong interaction between its functional groups and Zn^{2+}, homogenous ion flux is prompted, inducing uniform and dendrite-free Zn deposition.

5.1 Biomass-derived carbon as protective layer for Zn anode

One effective manner of protecting Zn by using biomass materials is to convert them into facile carbon coatings, where similar scenario of regulating interfacial reactions can be applied.

A biomass carbon coating obtained from corn flour was innovatively proposed on Zn anode, which had the advantages of low price, large SSA, good conductivity and outstanding chemical stability [137]. The porous structure of biomass-derived carbon can not only construct a consecutive conductive network with sufficient void space to promote the evenly distributed interface electric field, but also provide large SSA for adsorption, preferentially guiding Zn deposition in the void. A lightweight and flexible 3D carbon nanofiber architecture with uniform Zn seeds (CNF-Zn) was prepared from BC, which was synthesized by specific microorganisms, including *acetobacter*, *agrobacterium*, *rhizobium* and *sarcina* (Fig. 9(a)) [138]. The as-prepared 3D CNF-Zn with a porous interconnected network significantly decreases the local current density and the Zn seeds provide uniform nuclei to guide uniform Zn deposition. Benefiting from the synergistic effect of Zn seeds and 3D porous framework in the flexible CNF-Zn host, the electrochemical performance of the as-constructed ZIBs was significantly improved. The NaV_3O_8·1.5H_2O/CNF-Zn@Zn full battery further delivered a high and stable CE of 99.5% over 450 cycles and a long cycle life of over 500 cycles at 4 A·g^{-1} in the.

Porous biomass carbon (BCK) from carrot was artificially designed via a simple method to act as an *ex situ* surface coating on Zn anode [139]. BCK had a rich pore structure and zincophilic oxygen-containing functional groups, providing sufficient active sites. Together with large SSA, it could adsorb Zn^{2+} and lead to preferential nucleation on its surface, thus eliminating the tip effect and making the surface of Zn sheet uniform and flat. The MnO_2/BCK-7@Zn full cell delivered a capacity of 166.5 mAh·g^{-1} and the capacity retention rate of 61.5% after 1000 cycles at 1 A·g^{-1}, which was significantly higher than that of bare Zn assembled full cell.

5.2 Biomass as *ex situ* coating for Zn anode

On the other hand, biomaterials can be directly coated on Zn, where the retained hydrophilic/zincophilic functional groups can be utilized to manipulate interfacial reactions. Meanwhile, it offers an option to integrate the functions of gel electrolyte and protection layer.

An artificial SEI formed from cross-linked gelatin was introduced by coating the surface of Zn (Fig. 9(b)) [140]. Comparing to non-uniform, mossy deposited Zn on bare Zn, Zn deposits presented a much more uniform and dense manner with the gelatin layer. Employing electron back-scattered diffraction (EBSD), the absence of a coating layer led to isotropic and grain-independent deposition, supported by the extremely low indexing rate in EBSD at 1 mA·cm^{-2}, 1 mAh·cm^{-2}. In contrast, the coated Zn surface showed a much higher indexing rate, indicating the presence of micro-scale grains like those in pristine Zn, where intragranular anisotropy and isotropy were clearly differentiated.

Also, composite coating can be applied by introducing inorganic nanoparticles. An electric double layer (EDL) reconfiguration strategy was proposed by coating a SiO_2-SA hybrid film onto Zn surface (Zn@SiO_2-SA), to manipulate the distribution and chemical environment of Zn^{2+}, SO_4^{2-} and H_2O in the Helmholtz layer simultaneously (Fig. 9(c)) [141]. The tensile breaking stress of SiO_2@SA film (3.737 N) was larger than that of SA film (2.717 N), indicating the enhanced mechanical strength. In addition, the unique interfacial layer give rise to a uniform distribution of Zn^{2+} in the Helmholtz layer through solvation sheath modulation, as verified by COMSOL Multiphysics (Fig. 9(d)). DFT calculations and molecule dynamics (MD) simulations show that the SO_4^{2-} anions and free water are substantially reduced in the Helmholtz layer, effectively suppressing HER and the formation of by-products

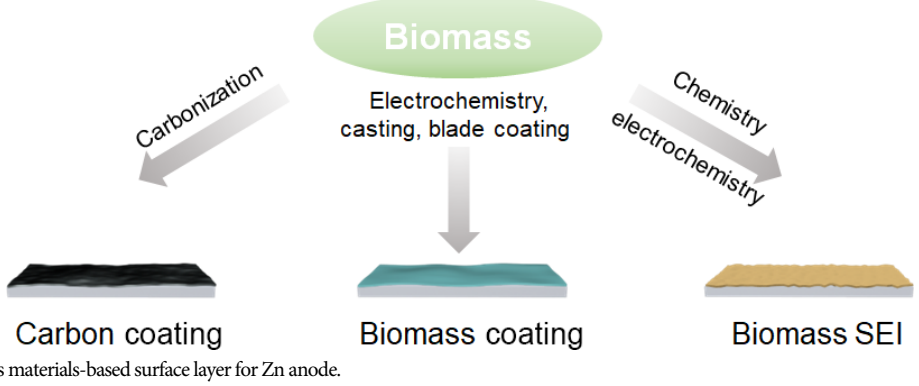

Figure 8 Roles of biomass materials-based surface layer for Zn anode.

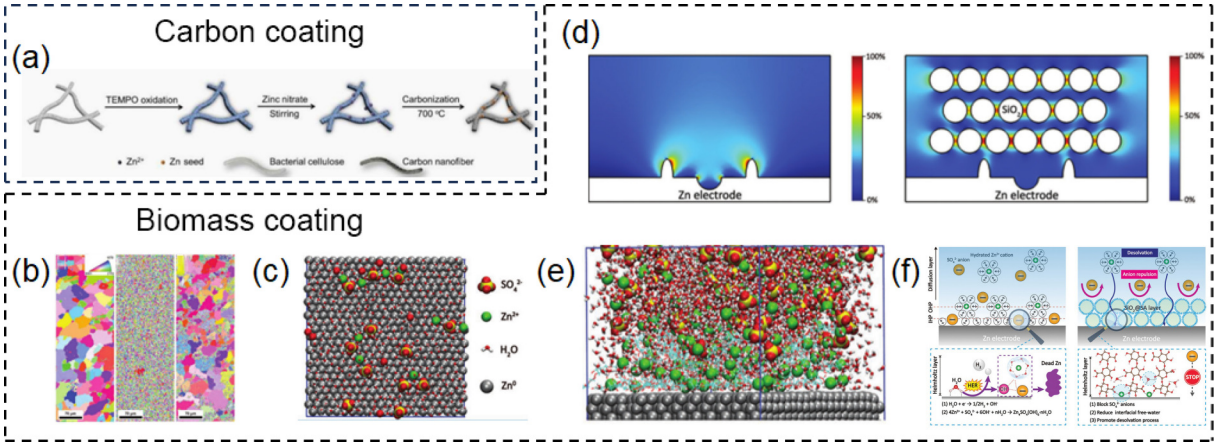

Figure 9 Biomass materials as protective layers for Zn anode: (a) Schematic diagram for the synthesis of CNF-Zn. Reproduced with permission from Ref. [138], © American Chemical Society 2023. (b) Surface EBSD maps of pristine Zn before plating, bare Zn after plating and coated Zn after plating. Reproduced with permission from Ref. [140], © Wiley-VCH GmbH 2021. (c) The cross-sectional image of simulated Helmholtz region. (d) COMSOL simulations of the Zn^{2+} flux on bare Zn and the Zn@SiO_2-SA electrode. (e) Image snapshots of Zn@SA interfaces through MD simulations. (f) Schematic illustrations of the EDL structure for bare Zn and Zn@SiO_2-SA electrode. Reproduced with permission from Ref. [141], © Wiley-VCH GmbH 2022.

through strong charge repulsion and H-bond fixing of free water (Fig. 9(e)). Thus, the reconfigured EDL not only ensures homogenous and fast Zn^{2+} transport kinetics for dendrite-free Zn deposition, but also eliminates interface parasitic side reactions (Fig. 9(f)).

Besides, fabrication of interface layer can be achieved by incorporating biopolymer in electrolyte as "additive". Chondroitin sulfate (CS), which enables the construction of an effective interface layer on Zn anode [142]. The presence of this effective interface layer guides the uniform migration to mitigate the "tip effect". Also, this interface layer effectively shields against direct contact between Zn and hydrate, thereby preventing side reactions. Simultaneously, the interaction between the $-SO_3H$ and Zn^{2+} is instrumental, which disrupts the solvation structure of Zn^{2+}, thus enabling Zn^{2+} to infiltrate the first solvation layer more uniformly. The assembled cell with CS additive achieved an ultrastable zinc plating/stripping performance for 4000 h at 1 mA·cm^{-2}, 1 mAh·cm^{-2} in Zn|Zn cell, with an ultrahigh service capacity of 4 Ah·cm^{-2}. Furthermore, the assembled MnO_2/Zn full cell achieved a stable cycling with a capacity retention of 75.0% after 10,000 cycles.

5.3 Biomass for construction of SEI on Zn

The weakly acidic nature of biopolymers and their derivatives, as well as strong complexing ability with zinc ions, facilitates the formation of so-based SEI on Zn via simple chemical routes.

An extremely simple and cost-effective method of protecting Zn was to soak Zn plate in TA solution, where ZnTA anticorrosive film formed on Zn surface (Fig. 10(a)) [143]. The strong interaction between Zn^{2+} and phenolic hydroxyl groups of TA contributes to the homogeneous ion flux, which facilitates uniform Zn deposition. In addition, high cohesion and compact microstructure of ZnTA anticorrosive film could reinforce the capacity of Zn anodes against the corrosion and inhibit HER remarkably.

By immersing commercial Zn foil into tartaric acid solution, an artificial interface protector with porous structure was introduced [146]. After soaking, the ratio of I (002)/ I (100) increased from 0.44 for bare Zn to 0.58 for tartaric acid solution@Zn, indicating the selective etching with more Zn (002) exposed. Meanwhile, the artificial layer endowed Zn with better anti-corrosion properties. Decreased charge transfer resistance (R_{ct}) by electrochemical impedance spectroscopy (EIS) facilitates fast charge transfer and speedy interfacial reaction kinetics, further leading to lower nucleation overpotential. From Arrhenius equation, lower E_a means fast desolvation process of hydrated Zn^{2+} ions, thus guaranteeing uniform Zn plating at 1 mA·cm^{-2}, 0.25 mAh·cm^{-2}. Inspired by the biomolecule-assisted cationic transport mechanism in nature, humic acid (HA, a natural ingredient of soil) was applied on the Zn surface (Zn@HA) to stabilize the electrolyte–anode interface (Fig. 10(b)) [144]. DFT calculations indicate that the interaction between Zn^{2+} and the segments of HA possibly facilitates the desolvation process. And the decreased contact angles indicated a better electrolyte wettability of Zn@HA. Zn@HA exhibited a lower HER current and corrosion current density, indicating the depressed side reactions on Zn. Thus, the symmetric cell with Zn@HA exhibited a long and stable Zn stripping/plating lifespan of 1900 h at 4.4 mA·cm^{-2}. A dense and uniform H_2O molecules-rich interphase of Zn^{2+} phytate (PAZn) was formed *in situ* on Zn surface by facile chemical treating with diluted phytic acid (PA) aqueous solution, endowing with effective coordination toward Zn^{2+} and shielding effect of crystal water (Fig. 10(c)) [145]. Benefiting from the strong interaction between phosphate groups and Zn^{2+}, PAZn interphase facilitates the desolvation of hydrated zinc ions and effectively alleviates water-induced side reactions, as well as regulating the Zn^{2+} flux through the interphase. Meanwhile, the Zn^{2+} diffusion coefficient showed orders of magnitude increase in the presence of crystal water due to its shielding effect, which ensures a facile deposition kinetics of Zn anode as verified by scanning electron microscope. And PAZn could endure Zn stripping/plating for 1200 h at 10 mA·cm^{-2}, 1 mAh·cm^{-2} and for 200 h at 10 mA·cm^{-2}, 3 mAh·cm^{-2}.

In addition, an artificial layer on Zn foil was fabricated via an electrochemical deposition method using $ZnCl_2$-cellulose electrolytes (Fig. 10(d)) [104]. Compared with bare Zn (−1.46 V vs. Ag/AgCl), the HER onset potential was shifted to −1.55 V, effectively suppressing hydrogen evolution. Also, the surface presented a positive shift of corrosion potential to ~ 0.88 V vs. Ag/AgCl with a lowered corrosion current of 0.37 mA·cm^{-2} (~ 1/2 of that for bare Zn), indicating its better corrosion resistance. The observed decrease in R_{ct} with the growth of surface layer by real-time EIS spectra suggested the favored interfacial kinetics, which

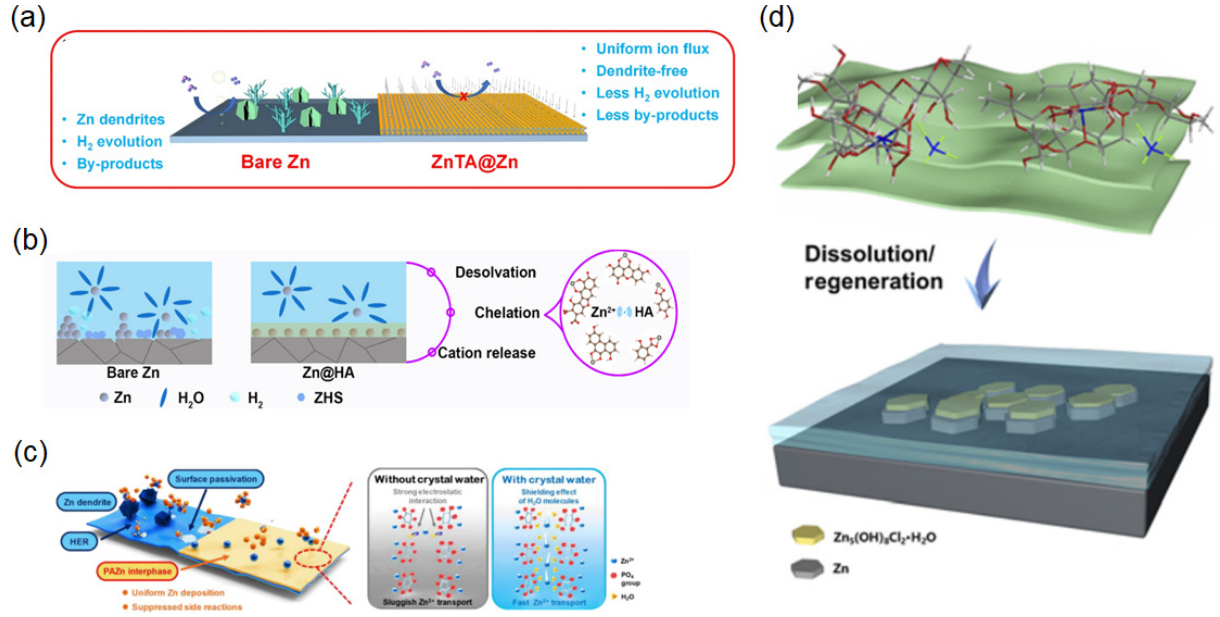

Figure 10 Biomass as *in situ* SEI for Zn anode: (a) The functions of ZnTA film. Reproduced with permission from Ref. [143], © Elsevier Ltd. 2022. (b) Schematic diagram of the interface evolution between the electrolyte and different anodes during deposition. Reproduced with permission from Ref. [144], © Elsevier B.V. 2023. (c) Schematic illustrations of Zn deposition process on bare Zn and PAZn@Zn and Zn^{2+} transport process in the PAZn framework in the absence/presence of crystal water. Reproduced with permission from Ref. [145], © American Chemical Society 2022. (d) Scheme of constructing an organic-dominant artificial SEI by ZCEs for Zn anode. Reproduced with permission from Ref. [104], © The Royal Society of Chemistry 2023.

could be achieved through the surface layer. Moreover, an improved transference number of ~ 0.59 was achieved by using the cell assembled with Zn-ZCE-2-3h in $Zn(OTf)_2$ compared with ~ 0.32 for that with bare Zn. It indicates the restriction of anion mobility of this organic-dominant surface, where electrostatic repulsion and steric hinderance may operate.

Hence, biomass materials exhibit their variety and flexibility in protecting Zn surface and manipulating the surface reactions on Zn. Being consistent with their functions in electrolytes or membranes, the zincophilic/hydrophilic groups in biomass play the central roles. It could be more challenging to identify the synergistic effects in such complex molecular systems.

6 Outlooks and perspectives

In conclusion, biomass materials are promising candidates as the key entities in ZESs, due to their multifunctionalities with increasing values. For cathode materials, novel meso/micro-porous structure, large surface area and enriched active sites of biomass-derived carbon can regulate the charge storage behavior. For electrolytes, the functional groups of biomass materials possess high affinity towards both zinc ions and water molecules, which can reshape the zinc solvation structure and tune the water activity. It influences the electrochemical stability and transport behavior of electrolytes. In addition, their uniqueness can be well displayed in gel electrolytes, but not limited to mechanical integrity, flexibility and self-healing. Also, the reaction interface will be regulated via the interaction between biomass and zinc ion, solvent molecules, in the form of either surface layers or separators. However, there are still important concerns need to be addressed before practical applications of biomass materials. The regulation on microstructure derived by biomass is still challenging. The operational mechanisms of biomass material on interface reactions are not clear. Meanwhile, the large-scale production/conversion of biomass material into key battery components is still in its early stage. Based on the above, we provide the following perspectives on the application of biomass materials in ZESs (Fig. 11).

Understanding of operational mechanisms. While biomass-based carbon, active materials (other than carbon materials) and binders collectively encompass the roles of biomass materials in cathodes, it is noteworthy that the enhancing mechanisms are not clear. Simultaneously, the intricate nature of the constituents within biomass materials contributes to the challenges in comprehending the underlying mechanisms. Thus, it is necessary to dedicate increasing efforts towards the exploration and comprehension of the operational mechanisms. In this regard, it is imperative to utilize advanced characterization and simulation tools to decouple the entangled effects.

From the perspective of biomass-derived carbon, it long remains as a great challenge to manipulate the microstructure of carbon materials derived from biomass, due to the diversity and dispersity of their compositions and molecular structures. On the other hand, it urges to explore the chemistry of controllable degradation from

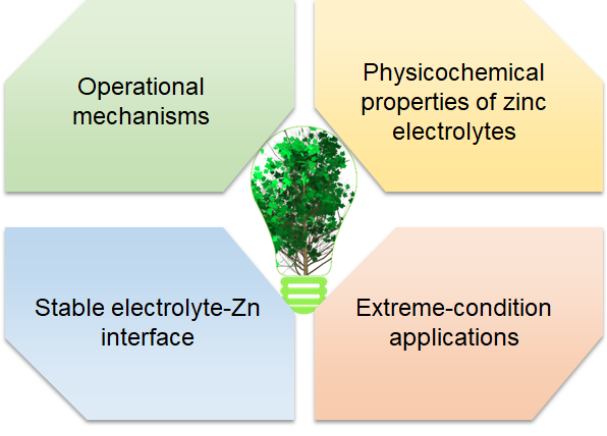

Figure 11 Future directions for biomass materials in ZESs.

biomass stock towards value-added molecular species. Furthermore, biomass, as well as biomass derived carbon, may further seek its significance in the newly developed Zn-based batteries. In parallel, carbon materials are promising stable cathodes for the development of novel electrolyte systems [147, 148]. Also, it exhibits great potential of demonstrating promising multi-electron charge transfer mechanisms, as in Zn-sulfur batteries.

Tuning physicochemical properties of zinc electrolytes. Except for cathode materials, biomass materials present their significant usage in electrolytes. Since the measured EW reflects the redox potential of Zn/Zn^{2+}, the depression of HER in biomass-based hydrogel is mostly claimed based on the depressed water activity. A quantitative measurement will be necessary when evaluating its large-scale application. Ion conductivities are typically high in hydrogel electrolytes, which infers a large content of water is included. It could be promising when transferred into eutectogel with a mixture of aqueous and non-aqueous solvents, which is being elaborated with more complex ion transport mechanisms.

Designing stable electrolyte-Zn interface. The regulation of ion flux may come from the interaction between functional groups and zinc ions. Meanwhile, the tunnels by the biomass cannot be overlooked. Long range ordering can present in biomass will definite repeated units, like cellulose and chitosan. The intermolecular interaction and transport behavior in the conduction tunnels by biomass warrant an insight.

Regarding Zn deposition, the formation of Zn texture has been reported for biomass-based electrolytes, e.g., CMC gel may induce Zn (101), cellulose in DES may induce Zn (002). So far, there is not a clear clue that which type of Zn texture will be favored by some specific type of biomass and more cases should be studied to provide a clear picture. This might be complex because of the complicated solvation structure in the biomass-based electrolytes, where both functional groups and conformation of polymer may play the roles. Also, multiple factors, like zinc concentration, anion and solvent, may blur the picture. From a practical point of view, DOD values for biomass-based electrolytes are not satisfied, typically below 10%. Thus, there is still a large room for the DOD improvement.

Developing novel ZESs for multi-functionalities. The functionalities associated with biomass components mainly include flexibility, self-healing and biodegradability. The first two characteristics have been well demonstrated in the flexible energy storage devices. Biodegradability might become future hotspot when implanting biocompatible aqueous batteries [149]. Furthermore, the structure of biomass with compatibility towards anti-freezing agents may make it become one powerful choice for working under extreme temperature. Moreover, the redox properties of biopolymers, e.g., polyphenol, deserve to be explored, which should be further discussed.

Therefore, we envision our minireview on the interdisciplinary role of biomass in ZESs may motivate advancing work towards sustainable energy technology.

Data availability

Not applicable.

Acknowledgements

X. T. Y. would like to acknowledge the support of College Students' Innovation and Entrepreneurship project. D. Y. would like to acknowledge the funding support from the 100 Talented Team of Hunan Province (XiangZu [2016] 91) and the Natural Science Foundation of Hunan Province (No. 2022JJ30613). M. Y. would like to acknowledge the Fundamental Research Funds for the Central Universities (No. YJ202280).

Declaration of competing interest

All the contributing authors report no conflict of interests in this work.

Author contribution statement

X. T. Y.: Data curation, writing manuscript. X. X. N.: Data curation, validation. C. K. T.: Data curation. Y. Y. X.: Data curation. Q. G. L.: Data curation. D. Y.: Project administration, funding acquisition, writing manuscript. M. Y.: Funding acquisition, writing manuscript. All the authors have approved the final manuscript.

Use of AI statement

None.

References

[1] Casola, F.; van der Sar, T.; Yacoby, A. Probing condensed matter physics with magnetometry based on nitrogen-vacancy centres in diamond. *Nat. Rev. Mater.* **2018**, *3*, 17088.

[2] Dong, H.; Tutusaus, O.; Liang, Y. L.; Zhang, Y.; Lebens-Higgins, Z.; Yang, W. L.; Mohtadi, R.; Yao, Y. High-power Mg batteries enabled by heterogeneous enolization redox chemistry and weakly coordinating electrolytes. *Nat. Energy* **2020**, *5*, 1043–1050.

[3] Fang, C. C.; Li, J. X.; Zhang, M. H.; Zhang, Y. H.; Yang, F.; Lee, J. Z.; Lee, M. H.; Alvarado, J.; Schroeder, M. A.; Yang, Y. Y. C. et al. Quantifying inactive lithium in lithium metal batteries. *Nature* **2019**, *572*, 511–515.

[4] Zhu, C. X.; Yang, J. R.; Zhang, J. W.; Wang, X. Q.; Gao, Y.; Wang, D. S.; Pan, H. G. Single-atom materials: The application in energy conversion. *Interdiscip. Mater.* **2024**, *3*, 74–86.

[5] Zhang, Y. D.; Sun, Y. J.; Wang, Q. Y.; Zhuang, Z. C.; Ma, Z. T.; Liu, L. M.; Wang, G. M.; Wang, D. S.; Zheng, X. S. Synergy of photogenerated electrons and holes toward efficient photocatalytic urea synthesis from CO_2 and N_2. *Angew. Chem., Int. Ed.* **2024**, *63*, e202405637.

[6] Qiu, W. B.; Qin, S. M.; Li, Y. B.; Cao, N.; Cui, W. R.; Zhang, Z. D.; Zhuang, Z. C.; Wang, D. S.; Zhang, Y. Overcoming electrostatic interaction via pulsed electroreduction for boosting the electrocatalytic urea synthesis. *Angew. Chem., Int. Ed.* **2024**, *63*, e202402684.

[7] Zhang, Z. D.; Zhu, J. X.; Chen, S. H.; Sun, W. M.; Wang, D. S. Liquid fluxional Ga single atom catalysts for efficient electrochemical CO_2 reduction. *Angew. Chem., Int. Ed.* **2023**, *62*, e202215136.

[8] Chen, S. H.; Ye, C. L.; Wang, Z. W.; Li, P.; Jiang, W. J.; Zhuang, Z. C.; Zhu, J. X.; Zheng, X. B.; Zaman, S.; Ou, H. H. et al. Selective CO_2 reduction to ethylene mediated by adaptive small-molecule engineering of copper-based electrocatalysts. *Angew. Chem., Int. Ed.* **2023**, *62*, e202315621.

[9] Ning, S. B.; Ou, H. H.; Li, Y. G.; Lv, C. C.; Wang, S. F.; Wang, D. S.; Ye, J. H. Co^0–$Co^{\delta+}$ interface double-site-mediated C–C coupling for the photothermal conversion of CO_2 into light olefins. *Angew. Chem., Int. Ed.* **2023**, *62*, e202302253.

[10] Blanc, L. E.; Kundu, D.; Nazar, L. F. Scientific challenges for the implementation of Zn-ion batteries. *Joule* **2020**, *4*, 771–799.

[11] Zhang, N.; Chen, X. Y.; Yu, M.; Niu, Z. Q.; Cheng, F. Y.; Chen, J.

Materials chemistry for rechargeable zinc-ion batteries. *Chem. Soc. Rev.* **2020**, *49*, 4203–4219.

[12] Cheng, X. B.; Zhang, R.; Zhao, C. Z.; Zhang, Q. Toward safe lithium metal anode in rechargeable batteries: A review. *Chem. Rev.* **2017**, *117*, 10403–10473.

[13] Wang, Y.; Wu, J.; Tang, S. H.; Yang, J. R.; Ye, C. L.; Chen, J.; Lei, Y. P.; Wang, D. S. Synergistic Fe–Se atom pairs as bifunctional oxygen electrocatalysts boost low-temperature rechargeable Zn-air battery. *Angew. Chem., Int. Ed.* **2023**, *62*, e202219191.

[14] Shi, W.; Lee, W. S. V.; Xue, J. M. Recent development of Mn-based oxides as zinc-ion battery cathode. *ChemSusChem* **2021**, *14*, 1634–1658.

[15] Yi, Z. H.; Chen, G. Y.; Hou, F.; Wang, L. Q.; Liang, J. Strategies for the stabilization of Zn metal anodes for Zn-ion batteries. *Adv. Energy Mater.* **2021**, *11*, 2003065.

[16] Sun, W.; Wang, F.; Hou, S.; Yang, C. Y.; Fan, X. L.; Ma, Z. H.; Gao, T.; Han, F. D.; Hu, R. Z.; Zhu, M. et al. Zn/MnO_2 battery chemistry with H^+ and Zn^{2+} coinsertion. *J. Am. Chem. Soc.* **2017**, *139*, 9775–9778.

[17] Wang, N.; Qiu, X.; Xu, J.; Huang, J. H.; Cao, Y. J.; Wang, Y. G. Cathode materials challenge varied with different electrolytes in zinc batteries. *ACS Mater. Lett.* **2022**, *4*, 190–204.

[18] Liu, A. N.; Wu, F.; Zhang, Y. X.; Zhou, J. H.; Zhou, Y. Z.; Xie, M. Insight on cathodes chemistry for aqueous zinc-ion batteries: From reaction mechanisms, structural engineering, and modification strategies. *Small* **2022**, *18*, 2201011.

[19] Lv, T. T.; Zhu, G. Y.; Dong, S. Y.; Kong, Q. Q.; Peng, Y.; Jiang, S.; Zhang, G. X.; Yang, Z. L.; Yang, S. Y.; Dong, X. C. et al. Co-intercalation of dual charge carriers in metal-ion-confining layered vanadium oxide nanobelts for aqueous zinc-ion batteries. *Angew. Chem., Int. Ed.* **2023**, *62*, e202216089.

[20] Zhu, G.; Zhang, H.; Lu, J.; Hou, Y.; Liu, P.; Dong, S.; Zhang, Y.; Dong, X. Recent advances in MXene-based anode materials for alkali metal-ion capacitors. *Mater. Today Sustain.* **2022**, *20*, 100226.

[21] Yin, J.; Zhang, W. L.; Alhebshi, N. A.; Salah, N.; Alshareef, H. N. Electrochemical zinc ion capacitors: Fundamentals, materials, and systems. *Adv. Energy Mater.* **2021**, *11*, 2100201.

[22] Xue, M. D.; Bai, J.; Wu, M. C.; He, Q. Q.; Zhang, Q. C.; Chen, L. Y. Carbon-assisted anodes and cathodes for zinc ion batteries: From basic science to specific applications, opportunities and challenges. *Energy Storage Mater.* **2023**, *62*, 102940.

[23] Liu, Y.; Wu, L. J. Recent advances of cathode materials for zinc-ion hybrid capacitors. *Nano Energy* **2023**, *109*, 108290.

[24] Luo, C.; Lei, H. Y.; Xiao, Y. Y.; Nie, X. X.; Li, Y. H.; Wang, Q.; Cai, W. L.; Dai, C. L.; Yao, M.; Zhang, Y. et al. Recent development in addressing challenges and implementing strategies for manganese dioxide cathodes in aqueous zinc ion batteries. *Energy Mater.* **2024**, *4*, 400036.

[25] Mu, X. Q.; Liu, S. L.; Zhang, M. Y.; Zhuang, Z. C.; Chen, D.; Liao, Y. R.; Zhao, H. Y.; Mu, S. C.; Wang, D. S.; Dai, Z. H. Symmetry-broken Ru nanoparticles with parasitic Ru-Co dual-single atoms overcome the volmer step of alkaline hydrogen oxidation. *Angew. Chem., Int. Ed.* **2024**, *63*, e202319618.

[26] Li, Y. P.; Niu, S. W.; Liu, P. G.; Pan, R. R.; Zhang, H. K.; Ahmad, N.; Shi, Y.; Liang, X.; Cheng, M. Y.; Chen, S. H. et al. Ruthenium nanoclusters and single atoms on α-MoC/N-doped carbon achieves low-input/input-free hydrogen evolution via decoupled/coupled hydrazine oxidation. *Angew. Chem., Int. Ed.* **2024**, *63*, e202316755.

[27] Han, A. L.; Sun, W. M.; Wan, X.; Cai, D. D.; Wang, X. J.; Li, F.; Shui, J. L.; Wang, D. S. Construction of Co_4 atomic clusters to Enable Fe-N_4 motifs with highly active and durable oxygen reduction performance. *Angew. Chem., Int. Ed.* **2023**, *62*, e202303185.

[28] Hu, Y. M.; Chao, T. T.; Li, Y. P.; Liu, P. G.; Zhao, T. H.; Yu, G.; Chen, C.; Liang, X.; Jin, H. L.; Niu, S. W. et al. Cooperative Ni(Co)-Ru-P sites activate dehydrogenation for hydrazine oxidation assisting self-powered H_2 production. *Angew. Chem., Int. Ed.* **2023**, *62*, e202308800.

[29] Wang, L. G.; Wu, J. B.; Wang, S. W.; Liu, H.; Wang, Y.; Wang, D. S. The reformation of catalyst: From a trial-and-error synthesis to rational design. *Nano Res.* **2024**, *17*, 3261–3301.

[30] Wang, Y.; Zheng, X. B.; Wang, D. S. Design concept for electrocatalysts. *Nano Res.* **2022**, *15*, 1730–1752.

[31] Zhu, P.; Xiong, X.; Wang, D. S. Regulations of active moiety in single atom catalysts for electrochemical hydrogen evolution reaction. *Nano Res.* **2022**, *15*, 5792–5815.

[32] Li, R. Z.; Wang, D. S. Understanding the structure–performance relationship of active sites at atomic scale. *Nano Res.* **2022**, *15*, 6888–6923.

[33] Zhang, X. M.; Deng, Z. W.; Xu, C. H. Y.; Deng, Y.; Jia, Y.; Luo, H.; Wu, H.; Cai, W. L.; Zhang, Y. Electrolyte engineering via competitive solvation structures for developing longevous zinc ion batteries. *Adv. Energy Mater.* **2023**, *13*, 2302749.

[34] Yang, Q.; Li, Q.; Liu, Z. X.; Wang, D. H.; Guo, Y.; Li, X. L.; Tang, Y. C.; Li, H. F.; Dong, B. B.; Zhi, C. Y. Dendrites in Zn-based batteries. *Adv. Mater.* **2020**, *32*, 2001854.

[35] Hao, J. N.; Li, X. L.; Zeng, X. H.; Li, D.; Mao, J. F.; Guo, Z. P. Deeply understanding the Zn anode behaviour and corresponding improvement strategies in different aqueous Zn-based batteries. *Energy Environ. Sci.* **2020**, *13*, 3917–3949.

[36] Zheng, J. X.; Archer, L. A. Controlling electrochemical growth of metallic zinc electrodes: Toward affordable rechargeable energy storage systems. *Sci. Adv.* **2021**, *7*, eabe0219.

[37] Zheng, X. B.; Yang, J. R.; Xu, Z. F.; Wang, Q. S.; Wu, J. B.; Zhang, E. H.; Dou, S. X.; Sun, W. P.; Wang, D. S.; Li, Y. D. Ru–Co pair sites catalyst boosts the energetics for the oxygen evolution reaction. *Angew. Chem., Int. Ed.* **2022**, *61*, e202205946.

[38] Yang, J. J.; Zhao, R.; Wang, Y. S.; Hu, Z. F.; Wang, Y. H.; Zhang, A. Q.; Wu, C.; Bai, Y. Insights on artificial interphases of Zn and electrolyte: Protection mechanisms, constructing techniques, applicability, and prospective. *Adv. Funct. Mater.* **2023**, *33*, 2213510.

[39] Zhou, M.; Chen, Y.; Fang, G. Z.; Liang, S. Q. Electrolyte/electrode interfacial electrochemical behaviors and optimization strategies in aqueous zinc-ion batteries. *Energy Storage Mater.* **2022**, *45*, 618–646.

[40] Zhang, Q.; Luan, J. Y.; Tang, Y. G.; Ji, X. B.; Wang, H. Y. Interfacial design of dendrite-free zinc anodes for aqueous zinc-ion batteries. *Angew. Chem., Int. Ed.* **2020**, *59*, 13180–13191.

[41] Chen, J. Y.; Qiao, X.; Han, X. R.; Zhang, J. H.; Wu, H. B.; He, Q.; Chen, Z. B.; Shi, L.; Wang, Y. Z.; Xie, Y. N. et al. Releasing plating-induced stress for highly reversible aqueous Zn metal anodes. *Nano Energy* **2022**, *103*, 107814.

[42] Zheng, J. X.; Zhu, G. Y.; Liu, X.; Xie, H. X.; Lin, Y. D.; Zeng, Y.; Zhang, Y. Z.; Gandi, A. N.; Qi, Z. B.; Wang, Z. C. et al. Simultaneous dangling bond and zincophilic site engineering of SiN_x protective coatings toward stable zinc anodes. *ACS Energy Lett.* **2022**, *7*, 4443–4450.

[43] Hao, Z. M.; Zhang, Y. F.; Hao, Z. K.; Li, G.; Lu, Y.; Jin, S.; Yang, G. J.; Zhang, S. H.; Yan, Z. H.; Zhao, Q. et al. Metal anodes with ultrahigh reversibility enabled by the closest packing crystallography for sustainable batteries. *Adv. Mater.* **2023**, *35*, 2209985.

[44] Zheng, J. X.; Zhao, Q.; Tang, T.; Yin, J. F.; Quilty, C. D.; Renderos, G. D.; Liu, X. T.; Deng, Y.; Wang, L.; Bock, D. C. et al. Reversible epitaxial electrodeposition of metals in battery anodes. *Science* **2019**, *366*, 645–648.

[45] Yuan, D.; Zhao, J.; Ren, H.; Chen, Y. Q.; Chua, R.; Jie, E. T. J.; Cai, Y.; Edison, E.; Manalastas Jr, W.; Wong, M. W. et al. Anion texturing towards dendrite-free Zn anode for aqueous rechargeable batteries. *Angew. Chem., Int. Ed.* **2021**, *60*, 7213–7219.

[46] Hu, W.; Ju, J. G.; Deng, N. P.; Liu, M. Y.; Liu, W. C.; Zhang, Y. X.; Fan, L. L.; Kang, W. M.; Cheng, B. W. Recent progress in tackling

Zn anode challenges for Zn ion batteries. *J. Mater. Chem. A* **2021**, *9*, 25750–25772.

[47] Wang, S. B.; Ran, Q.; Yao, R. Q.; Shi, H.; Wen, Z.; Zhao, M.; Lang, X. Y.; Jiang, Q. Lamella-nanostructured eutectic zinc-aluminum alloys as reversible and dendrite-free anodes for aqueous rechargeable batteries. *Nat. Commun.* **2020**, *11*, 1634.

[48] Wu, C.; Tan, H. T.; Huang, W. J.; Li, W. X.; Dinh, K. N.; Yan, C. S.; Wei, W. F.; Chen, L. B.; Yan, Q. Y. A new scalable preparation of metal nanosheets: Potential applications for aqueous Zn-ion batteries anode. *Adv. Funct. Mater.* **2020**, *30*, 2003187.

[49] Chen, Z. B.; Zhao, J.; He, Q.; Li, M. S.; Feng, S.; Wang, Y. Z.; Yuan, D.; Chen, J. Y.; Alshareef, H. N.; Ma, Y. W. Texture control of commercial Zn foils prolongs their reversibility as aqueous battery anodes. *ACS Energy Lett.* **2022**, *7*, 3564–3571.

[50] Pu, S. D.; Gong, C.; Tang, Y. T.; Ning, Z. Y.; Liu, J. L.; Zhang, S. M.; Yuan, Y.; Melvin, D.; Yang, S. X.; Pi, L. Q. et al. Achieving ultrahigh-rate planar and dendrite-free zinc electroplating for aqueous zinc battery anodes. *Adv. Mater.* **2022**, *34*, 2202552.

[51] Chen, Z. B.; Wu, Q.; Han, X. R.; Wang, C.; Chen, J. L.; Hu, T.; He, Q.; Zhu, X. Y.; Yuan, D.; Chen, J. Y. et al. Converting commercial Zn foils into single (002)-textured Zn with millimeter-sized grains for highly reversible aqueous zinc batteries. *Angew. Chem., Int. Ed.* **2024**, *63*, e202401507.

[52] Yu, A.; Zhang, W.; Joshi, N.; Yang, Y. Recent advances in anode design for mild aqueous Zn-ion batteries. *Energy Storage Mater.* **2024**, *64*, 103075.

[53] Cheng, Y.; Jiao, Y. C.; Wu, P. Y. Manipulating Zn 002 deposition plane with zirconium ion crosslinked hydrogel electrolyte toward dendrite free Zn metal anodes. *Energy Environ. Sci.* **2023**, *16*, 4561–4571.

[54] Li, X. W.; Ye, P.; Dou, A. C.; Jiang, Z. Y.; Naveed, A.; Zhou, Y.; Su, M. R.; Zhang, P. P.; Liu, Y. J. Nanoporous Nb_2O_5 coatings enabled long-life and deeply rechargeable zinc anodes for aqueous zinc-ion batteries. *J. Energy Storage* **2024**, *76*, 109874.

[55] Li, T.; Li, X.; Yang, H. F.; Zhou, Y.; Li, X. W.; Su, M. R.; Dou, A. C.; Zhang, P. P.; Wu, X. W.; Naveed, A. et al. Multifunctional optimization enabled by the space design of a nontoxic fluoride protective layer for dendrites-free and corrosion-resistant zinc anodes. *Mater. Today Energy* **2024**, *40*, 101513.

[56] Hu, B.; Xu, J.; Fan, Z. J.; Xu, C.; Han, S. C.; Zhang, J. X.; Ma, L. B.; Ding, B.; Zhuang, Z. C.; Kang, Q. et al. Covalent organic framework based lithium-sulfur batteries: Materials, interfaces, and solid-state electrolytes. *Adv. Energy Mater.* **2023**, *13*, 2203540.

[57] Wang, R.; Wu, Q. F.; Wu, M. J.; Zheng, J. X.; Cui, J.; Kang, Q.; Qi, Z. B.; Ma, J. D.; Wang, Z. C.; Liang, H. F. Interface engineering of Zn meal anodes using electrochemically inert Al_2O_3 protective nanocoatings. *Nano Res.* **2022**, *15*, 7227–7233.

[58] Liu, C. X.; Xie, X. S.; Lu, B. G.; Zhou, J.; Liang, S. Q. Electrolyte strategies toward better zinc-ion batteries. *ACS Energy Lett.* **2021**, *6*, 1015–1033.

[59] Verma, V.; Kumar, S.; Manalastas, W.; Srinivasan, M. Undesired reactions in aqueous rechargeable zinc ion batteries. *ACS Energy Lett.* **2021**, *6*, 1773–1785.

[60] Yang, W. H.; Yang, Y.; Yang, H. J.; Zhou, H. S. Regulating water activity for rechargeable zinc-ion batteries: Progress and perspective. *ACS Energy Lett.* **2022**, *7*, 2515–2530.

[61] Zhang, Y. J.; Chen, Z.; Qiu, H. Y.; Yang, W. H.; Zhao, Z. M.; Zhao, J. W.; Cui, G. L. Pursuit of reversible Zn electrochemistry: A time-honored challenge towards low-cost and green energy storage. *NPG Asia Mater.* **2020**, *12*, 4.

[62] Lv, Y. Q.; Xiao, Y.; Ma, L. T.; Zhi, C. Y.; Chen, S. M. Recent advances in electrolytes for "beyond aqueous" zinc-ion batteries. *Adv. Mater.* **2022**, *34*, 2106409.

[63] Zhu, Y. Z.; Fan, J. J.; Zhang, S.; Feng, Z. H.; Liu, C.; Zhu, R. B.; Liu, Y. J.; Guan, P. Y.; Li, M. Y.; Han, Z. J. et al. Long-life flexible mild Ag-Zn fibrous battery with bifunctional gel electrolyte. *Chem. Eng. J.* **2024**, *480*, 148334.

[64] Sun, C.; Zhang, W. D.; Qiu, D. P.; Tong, M. M.; Chen, Z. S.; Sun, S. H.; Lai, C.; Hou, Y. L. Practicable Zn metal batteries enabled by ultrastable ferromagnetic interface. *Sci. Bull.* **2023**, *68*, 2750–2759.

[65] Wu, C. P.; Sun, C.; Ren, K. X.; Yang, F. L.; Du, Y. X.; Gu, X. X.; Wang, Q. H.; Lai, C. 2-methyl imidazole electrolyte additive enabling ultra-stable Zn anode. *Chem. Eng. J.* **2023**, *452*, 139465.

[66] Zhu, Y. X.; Ge, M. Y.; Ma, F. C.; Wang, Q. H.; Huang, P.; Lai, C. Multifunctional electrolyte additives for better metal batteries. *Adv. Funct. Mater.* **2024**, *34*, 2301964.

[67] Liu, J. W.; Li, C. X.; Lv, Q. L.; Chen, D. H.; Zhao, J. L.; Xia, X. D.; Wu, Z. X.; Lai, J. P.; Wang, L. Reconstruction of electric double layer on the anode interface by localized electronic structure engineering for aqueous Zn ion batteries. *Adv. Energy Mater.* **2024**, *14*, 2401118.

[68] Lu, H. Y.; Hu, J. S.; Wei, X. J.; Zhang, K. Q.; Xiao, X.; Zhao, J. X.; Hu, Q.; Yu, J.; Zhou, G. M.; Xu, B. G. A recyclable biomass electrolyte towards green zinc-ion batteries. *Nat. Commun.* **2023**, *14*, 144435.

[69] Chen, W. S.; Yu, H. P.; Lee, S. Y.; Wei, T.; Li, J.; Fan, Z. J. Nanocellulose: A promising nanomaterial for advanced electrochemical energy storage. *Chem. Soc. Rev.* **2018**, *47*, 2837–2872.

[70] Sun, Z. H.; Fridrich, B.; De Santi, A.; Elangovan, S.; Barta, K. Bright side of lignin depolymerization: Toward new platform chemicals. *Chem. Rev.* **2018**, *118*, 614–678.

[71] Wang, C. Y.; Yokota, T.; Someya, T. Natural biopolymer-based biocompatible conductors for stretchable bioelectronics. *Chem. Rev.* **2021**, *121*, 2109–2146.

[72] Yang, Y. J.; Xiao, Y. Y.; Nie, X. X.; Yao, M.; Liang, H. F.; Yuan, D. Carbon materials in current zinc ion energy storage devices towards sustainability. *Carbon Res.* **2024**, *3*, 62.

[73] Yang, L.; Li, J. Q.; Zhou, Y. C.; Yao, J. F. Towards high-performance supercapacitors with cellulose-based carbon for zinc-ion storage. *J. Energy Storage* **2022**, *50*, 104252.

[74] Yu, P. F.; Zeng, Y.; Zeng, Y. X.; Dong, H. W.; Hu, H.; Liu, Y. L.; Zheng, M. T.; Xiao, Y.; Lu, X. H.; Liang, Y. R. Achieving high-energy-density and ultra-stable zinc-ion hybrid supercapacitors by engineering hierarchical porous carbon architecture. *Electrochim. Acta* **2019**, *327*, 134999.

[75] Zhao, L.; Jian, W. B.; Zhang, X. S.; Wen, F. W.; Zhu, J. H.; Huang, S.; Yin, J.; Lu, K.; Zhou, M. S.; Zhang, W. L. et al. Multi-scale self-templating synthesis strategy of lignin-derived hierarchical porous carbons toward high-performance zinc ion hybrid supercapacitors. *J. Energy Storage* **2022**, *53*, 105095.

[76] Zhao, J. Q.; Wu, W. L.; Jia, X. W.; Xia, T.; Li, Q. Y.; Zhang, J.; Wang, Q. H.; Zhang, W.; Lu, C. H. High-value utilization of biomass waste: From garbage floating on the ocean to high-performance rechargeable Zn-MnO_2 batteries with superior safety. *J. Mater. Chem. A* **2020**, *8*, 18198–18206.

[77] Zeng, G. L.; Wang, Y. Q.; Lou, X. M.; Chen, H.; Jiang, S. H.; Zhou, W. Vanadium oxide/carbonized chestnut needle composites as cathode materials for advanced aqueous zinc-ion batteries. *J. Energy Storage* **2024**, *77*, 109859.

[78] Jaikrajang, N.; Kao-Ian, W.; Muramatsu, T.; Chanajaree, R.; Yonezawa, T.; Al Balushi, Z. Y.; Kheawhom, S.; Cheacharoen, R. Impact of binder functional groups on controlling chemical reactions to improve stability of rechargeable zinc-ion batteries. *ACS Appl. Energy Mater.* **2021**, *4*, 7138–7147.

[79] Yang, G. S.; Huang, J. L.; Wan, X. H.; Zhu, Y. C.; Liu, B. B.; Wang, J. W.; Hiralal, P.; Fontaine, O.; Guo, Y. Z.; Zhou, H. A low cost, wide temperature range, and high energy density flexible quasi-solid-state zinc-ion hybrid supercapacitors enabled by sustainable cathode and electrolyte design. *Nano Energy* **2021**, *90*, 106500.

[80] Wang, H.; Wang, M.; Tang, Y. B. A novel zinc-ion hybrid

supercapacitor for long-life and low-cost energy storage applications. *Energy Storage Mater.* **2018**, *13*, 1–7.

[81] He, L.; Liu, Y.; Li, C. Y.; Yang, D. Z.; Wang, W. G.; Yan, W. Q.; Zhou, W. B.; Wu, Z. X.; Wang, L. L.; Huang, Q. H. et al. A low-cost Zn-based aqueous supercapacitor with high energy density. *ACS Appl. Energy Mater.* **2019**, *2*, 5835–5842.

[82] Li, Z. W.; Chen, D. H.; An, Y. F.; Chen, C. L.; Wu, L. Y.; Chen, Z. J.; Sun, Y.; Zhang, X. G. Flexible and anti-freezing quasi-solid-state zinc ion hybrid supercapacitors based on pencil shavings derived porous carbon. *Energy Storage Mater.* **2020**, *28*, 307–314.

[83] Li, X.; Hu, J. D.; Wu, M.; Guo, C. C.; Bai, L.; Li, J. M.; Li, Y. W.; Luo, D. H.; Duan, J. M.; Li, X. L. et al. Fabrication and morphological effect of waxberry-like carbon for high-performance aqueous zinc-ion electrochemical storage. *Carbon* **2023**, *205*, 226–235.

[84] Fan, W. J.; Ding, J.; Ding, J. N.; Zheng, Y. L.; Song, W. Q.; Lin, J. F.; Xiao, C. X.; Zhong, C.; Wang, H. L.; Hu, W. B. Identifying heteroatomic and defective sites in carbon with dual-ion adsorption capability for high energy and power zinc ion capacitor. *Nano-Micro Lett.* **2021**, *13*, 59.

[85] Du, X. Y.; Ma, Y. P.; Xie, X. B.; Jiang, H. Y.; Sun, X. Q.; Yang, X. Y.; Zhang, Y. P.; Hou, C. X.; Du, W. Preparation of two-dimensional porous nitrogen-oxygen co-doped recycled yeast cell wall derived-carbon matrix for high-performance zinc ion supercapacitors. *J. Energy Storage* **2024**, *82*, 110428.

[86] Wang, S. L.; Wang, Q.; Zeng, W.; Wang, M.; Ruan, L. M.; Ma, Y. N. A new free-standing aqueous zinc-ion capacitor based on MnO_2-CNTs cathode and MXene anode. *Nano-Micro Lett.* **2019**, *11*, 70.

[87] Ren, J. C.; Huang, Y. L.; Zhu, H.; Zhang, B. H.; Zhu, H. K.; Shen, S. H.; Tan, G. Q.; Wu, F.; He, H.; Lan, S. et al. Recent progress on MOF-derived carbon materials for energy storage. *Carbon Energy* **2020**, *2*, 176–202.

[88] Wang, H. Y.; Ye, W. Q.; Yang, Y.; Zhong, Y. J.; Hu, Y. Zn-ion hybrid supercapacitors: Achievements, challenges and future perspectives. *Nano Energy* **2021**, *85*, 105942.

[89] Zhao, X. J.; Hong, R. Z.; Lu, R. Y.; Chen, Y. J.; Yang, X. M. Sustainable synthesis of hierarchically porous hollow carbon spheres for enhanced zinc-ion hybrid supercapacitors. *ACS Appl. Energy Mater.* **2024**, *7*, 931–940.

[90] Javed, M. S.; Asim, S.; Najam, T.; Khalid, M.; Hussain, I.; Ahmad, A.; Assiri, M. A.; Han, W. H. Recent progress in flexible Zn-ion hybrid supercapacitors: Fundamentals, fabrication designs, and applications. *Carbon Energy* **2023**, *5*, e271.

[91] Wang, H.; Huang, J. X.; Wang, X. B.; Guo, Z. G.; Liu, W. M. *In-situ* construction of CNTs decorated titanium carbide on Ti mesh towards the synergetic improvement of energy storage properties for aqueous zinc ion capacitors. *ChemElectroChem* **2023**, *10*, e202201137.

[92] Zhang, J. J.; Wu, X.; Luo, S. H. MOF-derived porous carbon for zinc-ion hybrid capacitors with ultra-high energy density and long cycling life. *Batteries Supercaps* **2024**, *7*, e202400205.

[93] Wang, L.; Peng, M. K.; Chen, J. R.; Tang, X. N.; Li, L. B.; Hu, T.; Yuan, K.; Chen, Y. W. High energy and power zinc ion capacitors: A dual-ion adsorption and reversible chemical adsorption coupling mechanism. *ACS Nano* **2022**, *16*, 2877–2888.

[94] Li, L.; Jiang, L. L.; Qing, Y.; Zeng, Y. X.; Zhang, Z.; Xiao, L.; Lu, X. H.; Wu, Y. Q. Manipulating nickel oxides in naturally derived cellulose nanofiber networks as robust cathodes for high-performance Ni-Zn batteries. *J. Mater. Chem. A* **2020**, *8*, 565–572.

[95] Lv, W.; Shen, Z. L.; Li, X. D.; Meng, J. W.; Yang, W. J.; Ding, F.; Ju, X.; Ye, F.; Li, Y. M.; Lyu, X. F. et al. Discovering cathodic biocompatibility for aqueous Zn-MnO_2 battery: An integrating biomass carbon strategy. *Nano-Micro Lett* **2024**, *16*, 109.

[96] Patel, D.; Dharmesh, A.; Sharma, Y.; Rani, P.; Sharma, A. K. Hybrid electrolyte with biomass-derived carbon host for high-performance aqueous Zn-S battery. *Chem. Eng. J.* **2024**, *479*, 147722.

[97] Wang, K. N.; Wang, J. W.; Zhang, Z. Q.; Zhang, W. L.; Fu, F.; Du, Y. P. Pitch-derived 3D amorphous carbon encapsulated sulfur-rich cathode for aqueous Zn-S batteries. *Sci. China Chem.* **2023**, *66*, 2711–2718.

[98] Zhao, S. F.; Wu, X. S.; Zhang, J. L.; Li, C. J.; Cui, Z. X.; Hu, W. H.; Ma, R. G.; Li, C. M. Biomass-derived porous carbon with single-atomic cobalt toward high-performance aqueous zinc-sulfur batteries at room temperature. *Journal of Energy Chemistry* **2024**, *95*, 325–335.

[99] Wang, X. R.; Wang, Y. L.; Naveed, A.; Li, G. T.; Zhang, H. W.; Zhou, Y.; Dou, A. C.; Su, M. R.; Liu, Y. J.; Guo, R. Q. et al. Magnesium ion doping and micro-structural engineering assist $NH_4V_4O_{10}$ as a high-performance aqueous zinc ion battery cathode. *Adv. Funct. Mater.* **2023**, *33*, 2306205.

[100] Liu, Y.; Liu, Y.; Wu, X.; Cho, Y. R. General carbon modification avenue to construct highly stable V_2O_5 electrodes for aqueous zinc-ion batteries. *ACS Sustainable Chem. Eng.* **2023**, *11*, 13298–13305.

[101] Cheng, H. H.; Zhang, Y.; Cai, X. X.; Liu, C. F.; Wang, Z. W.; Ye, H.; Pan, Y. L.; Jia, D. Z.; Lin, H. Boosting zinc storage performance of Li_3VO_4 cathode material for aqueous zinc ion batteries via carbon-incorporation: A study combining theory and experiment. *Small* **2024**, *20*, 2305762.

[102] Yang, W.; Yang, Z.; Wang, J.; Lu, W.; Wang, W. H. A bean catching double pigeons: Sonication assisted modification of Nb_2C MXenes composites by O-doping porous biomass-carbons for supercapacitors and zinc-ion batteries. *J. Energy Storage* **2023**, *65*, 107334.

[103] Huang, H. J.; Yun, J. W.; Feng, H.; Tian, T.; Xu, J. W.; Li, D. L.; Xia, X.; Yang, Z. H.; Zhang, W. X. Towards high-performance zinc anode for zinc ion hybrid capacitor: Concurrently tailoring hydrodynamic stability, zinc deposition and solvation structure via electrolyte additive. *Energy Storage Mater.* **2023**, *55*, 857–866.

[104] Li, X.; Yao, H.; Li, Y. H.; Liu, X. J.; Yuan, D.; Chen, Y. Q.; Wong, M. W.; Zhang, Y. Z.; Zhang, H. T. Cellulose-complexing strategy induced surface regulation towards ultrahigh utilization rate of Zn. *J. Mater. Chem. A* **2023**, *11*, 14720–14727.

[105] Yang, W.; Yang, W.; Zeng, J. M.; Chen, Y. L.; Huang, Y. F.; Liu, J.; Gan, J. Y.; Li, T. Z.; Zhang, H.; Zhong, L. X. et al. Biopolymer-based gel electrolytes for electrochemical energy storage: Advances and prospects. *Prog. Mater. Sci.* **2024**, *144*, 101264.

[106] Chen, M. F.; Chen, J. Z.; Zhou, W. J.; Han, X.; Yao, Y. G.; Wong, C. P. Realizing an all-round hydrogel electrolyte toward environmentally adaptive dendrite-free aqueous Zn-MnO_2 batteries. *Adv. Mater.* **2021**, *33*, 2007559.

[107] Zhang, Q. C.; Li, C. W.; Li, Q. L.; Pan, Z. H.; Sun, J.; Zhou, Z. Y.; He, B.; Man, P.; Xie, L. Y.; Kang, L. X. et al. Flexible and high-voltage coaxial-fiber aqueous rechargeable zinc-ion battery. *Nano Lett.* **2019**, *19*, 4035–4042.

[108] Zhang, X. F.; Ma, X. F.; Hou, T.; Guo, K. C.; Yin, J. Y.; Wang, Z. G.; Shu, L.; He, M.; Yao, J. F. Inorganic salts induce thermally reversible and anti-freezing cellulose hydrogels. *Angew. Chem., Int. Ed.* **2019**, *58*, 7366–7370.

[109] Tang, Y.; Liu, C. X.; Zhu, H. R.; Xie, X. S.; Gao, J. W.; Deng, C. B.; Han, M. M.; Liang, S. Q.; Zhou, J. Ion-confinement effect enabled by gel electrolyte for highly reversible dendrite-free zinc metal anode. *Energy Storage Mater.* **2020**, *27*, 109–116.

[110] Xie, X. S.; Li, J. J.; Xing, Z. Y.; Lu, B. G.; Liang, S. Q.; Zhou, J. Biocompatible zinc battery with programmable electro-cross-linked electrolyte. *Natl. Sci. Rev.* **2023**, *10*, nwac281.

[111] Zhang, B. Y.; Qin, L. P.; Fang, Y.; Chai, Y. Z.; Xie, X. S.; Lu, B. G.; Liang, S. Q.; Zhou, J. Tuning Zn^{2+} coordination tunnel by

hierarchical gel electrolyte for dendrite-free zinc anode. *Sci. Bull.* **2022**, *67*, 955–962.

[112] Liu, Q.; Chen, R. P.; Xu, L.; Liu, Y.; Dai, Y. H.; Huang, M.; Mai, L. Steric molecular combing effect enables ultrafast self-healing electrolyte in quasi-solid-state zinc-ion batteries. *ACS Energy Lett.* **2022**, *7*, 2825–2832.

[113] Cao, G. H.; Zhao, L.; Ji, X. W.; Peng, Y. Y.; Yu, M. M.; Wang, X. Y.; Li, X. Y.; Ran, F. "Salting out" in Hofmeister effect enhancing mechanical and electrochemical performance of amide-based hydrogel electrolytes for flexible zinc-ion battery. *Small* **2023**, *19*, 2207610.

[114] Sun, L.; Yao, Y. Q.; Dai, L. X.; Jiao, M. L.; Ding, B. F.; Yu, Q. M.; Tang, J.; Liu, B. L. Sustainable and high-performance Zn dual-ion batteries with a hydrogel-based water-in-salt electrolyte. *Energy Storage Mater.* **2022**, *47*, 187–194.

[115] Li, C. P.; Xie, X. S.; Liu, H.; Wang, P. J.; Deng, C. B.; Lu, B. G.; Zhou, J.; Liang, S. Q. Integrated 'all-in-one' strategy to stabilize zinc anodes for high-performance zinc-ion batteries. *Natl. Sci. Rev.* **2022**, *9*, nwab177.

[116] Yang, L. Y.; Song, L.; Feng, Y.; Cao, M. J.; Zhang, P. C.; Zhang, X. F.; Yao, J. F. Zinc ion trapping in a cellulose hydrogel as a solid electrolyte for a safe and flexible supercapacitor. *J. Mater. Chem. A* **2020**, *8*, 12314–12318.

[117] Dong, H. B.; Li, J. W.; Zhao, S. Y.; Jiao, Y. D.; Chen, J. T.; Tan, Y. S.; Brett, D. J. L.; He, G. J.; Parkin, I. P. Investigation of a biomass hydrogel electrolyte naturally stabilizing cathodes for zinc-ion batteries. *ACS Appl. Mater. Interfaces* **2021**, *13*, 745–754.

[118] Liu, Q. Q.; Xia, C. F.; He, C. H.; Guo, W.; Wu, Z. P.; Li, Z.; Zhao, Q.; Xia, B. Y. Dual-network structured hydrogel electrolytes engaged solid-state rechargeable Zn-air/iodide hybrid batteries. *Angew. Chem., Int. Ed.* **2022**, *61*, e202210567.

[119] Almenara, N.; Gueret, R.; Huertas-Alonso, A. J.; Veettil, U. T.; Sipponen, M. H.; Lizundia, E. Lignin-chitosan gel polymer electrolytes for stable Zn electrodeposition. *ACS Sustainable Chem. Eng.* **2023**, *11*, 2283–2294.

[120] Zhang, S. L.; Yu, N. S.; Zeng, S.; Zhou, S. S.; Chen, M. H.; Di, J. T.; Li, Q. W. An adaptive and stable bio-electrolyte for rechargeable Zn-ion batteries. *J. Mater. Chem. A* **2018**, *6*, 12237–12243.

[121] Huang, Y.; Zhang, J. Y.; Liu, J. W.; Li, Z. X.; Jin, S. Y.; Li, Z. G.; Zhang, S. D.; Zhou, H. Flexible and stable quasi-solid-state zinc ion battery with conductive guar gum electrolyte. *Mater. Today Energy* **2019**, *14*, 100349.

[122] Han, Q.; Chi, X. W.; Zhang, S. M.; Liu, Y. Z.; Zhou, B.; Yang, J. H.; Liu, Y. Durable, flexible self-standing hydrogel electrolytes enabling high-safety rechargeable solid-state zinc metal batteries. *J. Mater. Chem. A* **2018**, *6*, 23046–23054.

[123] Li, H. F.; Han, C. P.; Huang, Y.; Huang, Y.; Zhu, M. S.; Pei, Z. X.; Xue, Q.; Wang, Z. F.; Liu, Z. X.; Tang, Z. J. et al. An extremely safe and wearable solid-state zinc ion battery based on a hierarchical structured polymer electrolyte. *Energy Environ. Sci.* **2018**, *11*, 941–951.

[124] Yang, Z. F.; Zhang, Q.; Wu, T. Q.; Li, Q. K.; Shi, J. M.; Gan, J. Q.; Xiang, S. E.; Wang, H.; Hu, C.; Tang, Y. G. et al. Thermally healable electrolyte–electrode interface for sustainable quasi-solid zinc-ion batteries. *Angew. Chem., Int. Ed.* **2024**, *63*, e202317457.

[125] Wang, J. W.; Huang, Y.; Liu, B. B.; Li, Z. X.; Zhang, J. Y.; Yang, G. S.; Hiralal, P.; Jin, S. Y.; Zhou, H. Flexible and anti-freezing zinc-ion batteries using a guar-gum/sodium-alginate/ethylene-glycol hydrogel electrolyte. *Energy Storage Mater.* **2021**, *41*, 599–605.

[126] Zhou, J. J.; Zhang, R. H.; Xu, R.; Li, Y.; Tian, W.; Gao, M.; Wang, M.; Li, D. W.; Liang, X.; Xie, L. et al. Super-assembled hierarchical cellulose aerogel-gelatin solid electrolyte for implantable and biodegradable zinc ion battery. *Adv. Funct. Mater.* **2022**, *32*, 2111406.

[127] Xiang, Z. P.; Li, Y. Y.; Cheng, X. J.; Yang, C.; Wang, K. P.; Zhang, Q.; Wang, L. Lean-water hydrogel electrolyte with improved ion conductivity for dendrite-free zinc-ion batteries. *Chem. Eng. J.* **2024**, *490*, 151524.

[128] Liu, X. J.; Li, X.; Yang, X. T.; Lu, J. Q.; Zhang, X.; Yuan, D.; Zhang, Y. Z. Influence of water on gel electrolytes for zinc-ion batteries. *Chem.—Asian J.* **2023**, *18*, e202201280.

[129] Kang, Q.; Zhuang, Z. C.; Liu, Y. J.; Liu, Z. H.; Li, Y.; Sun, B.; Pei, F.; Zhu, H.; Li, H. F.; Li, P. L. et al. Engineering the structural uniformity of gel polymer electrolytes via pattern-guided alignment for durable, safe solid-state lithium metal batteries. *Adv. Mater.* **2023**, *35*, 2303460.

[130] Wang, Y. H.; Zhang, Y. G.; Yu, W. Y.; Chen, F.; Ma, T. Y.; Huang, H. W. Single-atom catalysts for energy conversion. *J. Mater. Chem. A* **2023**, *11*, 2568–2594.

[131] Kang, Q.; Li, Y.; Zhuang, Z. C.; Yang, H. J.; Luo, L. X.; Xu, J.; Wang, J.; Guan, Q. H.; Zhu, H.; Zuo, Y. Z. et al. Engineering a dynamic solvent-phobic liquid electrolyte interphase for long-life lithium metal batteries. *Adv. Mater.* **2024**, *36*, 2308799.

[132] Yang, X. P.; Wu, W. L.; Liu, Y. Z.; Lin, Z. R.; Sun, X. Q. Chitosan modified filter paper separators with specific ion adsorption to inhibit side reactions and induce uniform Zn deposition for aqueous Zn batteries. *Chem. Eng. J.* **2022**, *450*, 137902.

[133] Zhou, W. J.; Chen, M. F.; Tian, Q. H.; Chen, J. Z.; Xu, X. W.; Wong, C. P. Cotton-derived cellulose film as a dendrite-inhibiting separator to stabilize the zinc metal anode of aqueous zinc ion batteries. *Energy Storage Mater.* **2022**, *44*, 57–65.

[134] Yuan, D.; Manalastas, W.; Zhang, L. P.; Chan, J. J.; Meng, S. Z.; Chen, Y. Q.; Srinivasan, M. Lignin@Nafion membranes forming Zn solid-electrolyte interfaces enhance the cycle life for rechargeable zinc-ion batteries. *ChemSusChem* **2019**, *12*, 4889–4900.

[135] Qin, H. Y.; Chen, W. J.; Kuang, W.; Hu, N.; Zhang, X. Y.; Weng, H. F.; Tang, H.; Huang, D.; Xu, J.; He, H. B. A nature-inspired separator with water-confined and kinetics-boosted effects for sustainable and high-utilization Zn metal batteries. *Small* **2023**, *19*, 2300130.

[136] Huang, Z. E.; Yang, S. C.; Zhang, Y.; Zhang, Y. X.; Xue, R. R.; Ma, Y.; Wang, Z. H. Ultrathin reed membranes: Nature's intimate ion-regulation skins safeguarding zinc metal anodes in aqueous batteries. *Adv. Energy Mater.* **2024**, *14*, 2400033.

[137] Ou, Z. N.; Liu, Q. N.; Wang, Y. X.; Wu, G. J. Biomass carbon modified zinc anode for rechargeable aqueous batteries. *Int. J. Electrochem. Sci.* **2022**, *17*, 220924.

[138] Wang, J. H.; Chen, L. F.; Dong, W. X.; Zhang, K. L.; Qu, Y. F.; Qian, J. W.; Yu, S. H. Three-dimensional zinc-seeded carbon nanofiber architectures as lightweight and flexible hosts for a highly reversible zinc metal anode. *ACS Nano* **2023**, *17*, 19087–19097.

[139] Zheng, W. J.; Xie, H. B.; Zhu, L.; Zhou, H.; Zhang, K. Elaborate artificial construction of porous biomass carbon interfacial layer on the surface of zinc anode toward high performance aqueous zinc-ion batteries. *J. Energy Storage* **2024**, *76*, 109808.

[140] Shin, J.; Lee, J.; Kim, Y.; Park, Y.; Kim, M.; Choi, J. W. Highly reversible, grain-directed zinc deposition in aqueous zinc ion batteries. *Adv. Energy Mater.* **2021**, *11*, 2100676.

[141] Yang, Y.; Hua, H. M.; Lv, Z. H.; Zhang, M. H.; Liu, C. Y.; Wen, Z. P.; Xie, H. D.; He, W. D.; Zhao, J. B.; Li, C. C. Reconstruction of electric double layer for long-life aqueous zinc metal batteries. *Adv. Funct. Mater.* **2023**, *33*, 2212446.

[142] Yang, J. Q.; Qiu, M. J.; Zhu, M. N.; Weng, C. C.; Li, Y.; Sun, P.; Mai, W.; Xu, M.; Pan, L. K.; Li, J. L. Biomacromolecule guiding construction of effective interface layer for ultra-stable zinc anode. *Energy Storage Mater.* **2024**, *67*, 103287.

[143] Zhang, P. F.; Wu, Z. Z.; Zhang, S. J.; Liu, L. Y.; Tian, Y. H.; Dou, Y. H.; Lin, Z.; Zhang, S. Q. Tannin acid induced anticorrosive film toward stable Zn-ion batteries. *Nano Energy* **2022**, *102*, 107721.

[144] Deng, C. B.; Li, Y.; Liu, S. J.; Yang, J. L.; Huang, B. L.; Liu, J. P.; Huang, J. Q. Nature-inspired interfacial engineering for highly stable Zn metal anodes. *Energy Storage Mater.* **2023**, *58*, 279–286.

[145] Jin, H. R.; Dai, S. M.; Zhu, Z. H.; Luo, Y. X.; Qi, B.; Liu, K. S.; Wu, T.; Zhuang, X. Y.; Zhou, J.; Huang, L. Crystal water boosted Zn^{2+} transfer kinetics in artificial solid electrolyte interphase for high-rate and durable zn anodes. *ACS Appl. Energy Mater.* **2022**, *5*, 10581–10590.

[146] Chen, X. H.; Shi, X. D.; Ruan, P. C.; Tang, Y.; Sun, Y. Y.; Wong, W. Y.; Lu, B. G.; Zhou, J. Construction of an artificial interfacial layer with porous structure toward stable zinc-metal anodes. *Small Sci.* **2023**, *3*, 2300007.

[147] Liu, H. W.; Chen, C. Y.; Yang, H.; Wang, Y.; Zou, L. L.; Wei, Y. S.; Jiang, J. L.; Guo, J. C.; Shi, W.; Xu, Q. et al. A zinc-dual-halogen battery with a molten hydrate electrolyte. *Adv. Mater.* **2020**, *32*, 2004553.

[148] Yin, J.; Zhang, W. L.; Wang, W. X.; Alhebshi, N. A.; Salah, N.; Alshareef, H. N. Electrochemical zinc ion capacitors enhanced by redox reactions of porous carbon cathodes. *Adv. Energy Mater.* **2020**, *10*, 2001705.

[149] Liu, Z. X.; Chen, Z. Z.; Lei, S. R.; Lu, B. G.; Liang, S. Q.; Li, J. J.; Zhou, J. Validating operating stability and biocompatibility toward safer zinc-based batteries. *Adv. Mater.* **2024**, *36*, 2308836.

[150] Lu, Y. Y.; Li, Z. W.; Bai, Z. Y.; Mi, H. Y.; Ji, C. C.; Pang, H.; Yu, C.; Qiu, J. S. High energy-power Zn-ion hybrid supercapacitors enabled by layered B/N co-doped carbon cathode. *Nano Energy* **2019**, *66*, 104132.